PHOTONICS Research

Open-ended exploration of ultrashort pulse lasers: an innovative design strategy for devices based on 2D materials

Qing Wu,[1] Gang Zhao,[1] Haibin Wu,[1] and Meng Zhang[2,*]

[1]Heilongjiang Province Key Laboratory of Laser Spectroscopy Technology and Application, Harbin University of Science and Technology, Harbin 150080, China
[2]School of Electronic and Information Engineering, Beihang University, Beijing 100191, China
*Corresponding author: mengzhang10@buaa.edu.cn

Received 26 January 2023; revised 24 March 2023; accepted 18 April 2023; posted 21 April 2023 (Doc. ID 483172); published 23 June 2023

Ultrashort pulse lasers have vital significance in the field of ultrafast photonics. A saturable absorber (SA) as the core device to generate ultrashort pulses has innovative design strategies; the most interesting of which is the integration strategy based on 2D materials. This review presents recent advances in the optoelectronic properties of 2D materials and in the way the materials are prepared, characterized, and integrated into devices. We have done a comprehensive review of the optical properties of materials and material-based devices and their current development in the field of fiber lasers and solid-state lasers. Finally, we offer a look at future applications for 2D materials in ultrafast lasers and their prospects.

https://doi.org/10.1364/PRJ.483172

1. INTRODUCTION

Ultrafast pulses have extensive applications in nonlinear imaging and microscopy [1,2], material processing [3], terahertz spectrometers [4], and supercontinuum generation [5]. After the first ultrafast laser, the Kerr-lens mode-locked Ti:sapphire laser was developed in the 1990s [6], scientists' interest in ultrafast mechanisms dramatically increased. The key device to generate an ultrashort pulse light source [7,8] is the saturable absorber (SA). SA devices have attracted the attention of scientists because of their simple, economical construction and the fact that they are a key factor influencing the excellent output parameters of the lasers. In the business field, semiconductor SA mirrors (SESAMs) have been commonly used as SAs [9,10], and SESAMs were rapidly developed in both solid-state lasers and fiber lasers over the past decades. There are, however, some deficiencies: SESAMs are incapable of mode-locking in a wide wavelength range and problems occur that include a narrow operating bandwidth, long recovery time, difficult modulation depth, and low optical damage threshold. Therefore, it is a far-reaching task to explore new SA materials to achieve ultrafast pulses.

Experts in ultrafast optics favor 2D materials with high optical nonlinear polarization coefficients, ultrafast carrier dynamics, and broad operating wavelengths. Atomically layered materials that can be a single layer to a few layers, which have strong intralayer covalent bonds and weak interlayer van der Waals forces are examples of 2D materials. In the absence of interference from interlayer interactions, the motion of electrons is confined to the 2D system, which leads to 2D materials with many novel physical properties. In 2004, Novoselov *et al.* at the University of Manchester succeeded in stripping graphene, a layered material composed of individual carbon atoms [11]. This discovery acted as a guiding light and caused a worldwide research boom in various graphene fields because of its rich physical properties. Since then, scientists have been enthusiastic about the exploration of 2D materials and, stimulated by the success of graphene, other layered materials such as topological insulators (TIs), transition metal dichalcogenides (TMDs), black phosphorus (BP), MXenes, heterostructures, and graphdiyne have been discovered for applications, thus enriching the family of 2D layered materials. In 2009, in a review of carbon nanotubes for ultrafast photonics, Hasan *et al.* proposed that graphene has good SA properties and a wider range of operation and tunability compared to single-wall nanotubes [12]. Bao *et al.* successfully obtained ultrashort pulse outputs for fiber lasers based on graphene [13]. Sun *et al.* achieved mode-locked fiber lasers with pulse durations on the order of 460 femtoseconds based on graphene SAs [14]. In 2012, they demonstrated that inkjet printing is a feasible method to fabricate graphene devices over large areas and that the method can be used to print on any substrate. This study not only paved the way for flexible and transparent graphene devices, but also greatly advanced the application of graphene materials in ultrafast photonics [15]. These early explorations drove the rapid development of graphene in ultrafast photonics.

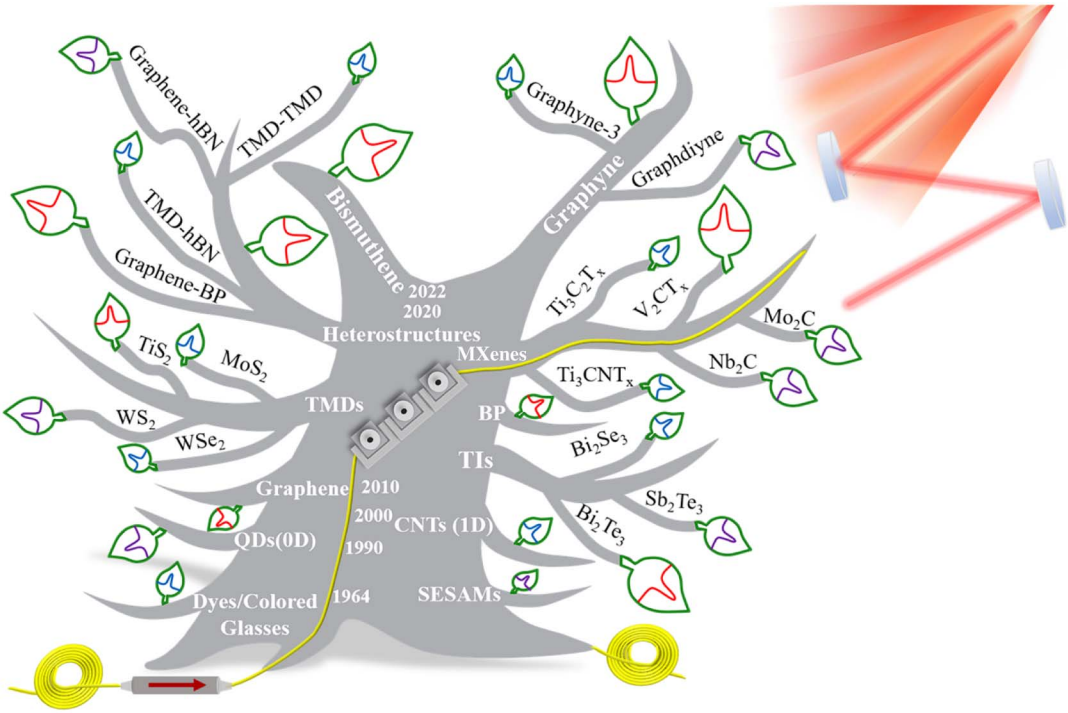

Fig. 1. Evolution of SAs based on materials (0D, 1D, and 2D) in the field of mode-locked lasers.

Inspired by graphene research, researchers have applied a variety of 2D materials to lasers, entering the era of combining 2D materials with ultrafast lasers. Among ultrafast lasers, mode-locked lasers can produce pulse widths in the picosecond (ps) range and even the femtosecond (fs) range [13,16], which is an important field to explore. Figure 1 summarizes the research done on SAs based on materials (0D, 1D, and 2D) in mode-locked fiber lasers and mode-locked solid-state lasers. However, 2D materials are more able to make the output parameters of mode-locked lasers even better, so this review focuses on summarizing mode-locked lasers. As the research continues to progress, the preparation and application of mode-locked lasers at 1 μm have become more and more mature and much excellent research has been done [17,18] that has led to the practical and commercialization stage of ultrashort pulse lasers. The first successful implementation of mode-locked lasers based on SAs of 2D materials was at 1.5 μm. That implementation was followed by many other studies on mode-locked lasers based on different materials and 1.5 μm received more attention. There are many device integration strategies and comprehensive comparisons of laser performance output. In addition, the relatively slow development of mode-locked lasers at 2 μm means that there is still much research to be done. Therefore, based on the research hotspots and development speed, in this paper we have focused on the 1.5 μm and 2 μm bands of mode-locked lasers based on 2D materials.

This review offers an in-depth look at the electrical and optical properties of 2D materials, preparation strategies, and device integration strategies, and describes nonlinear testing of 2D materials possessing unique properties. Different 2D materials also are discussed as SAs for mode-locked lasers, and the performance indexes of lasers such as the operating wavelength, pulse width, repetition frequency, and peak power are discussed. In addition, the mode-locked laser output characteristics of graphdiyne, a currently popular 2D material, are discussed in terms of its use as an SA. Ultimately, the development trend of ultrafast mode-locked lasers based on 2D materials is discussed and related conclusions are given. Given the importance of nonlinear optical materials in the field of ultrafast photonics, 2D nanomaterials have great promise to advance ultrafast laser technology.

2. FUNDAMENTALS OF 2D MATERIALS APPLIED IN ULTRAFAST MODE-LOCKED LASERS

A. Electrical and Optical Properties of 2D Materials

Graphene is the first 2D material to be discovered, and it is a flattened single layer of carbon atoms arranged in a tightly packed 2D honeycomb lattice, as shown in Fig. 2(a) [19]. It is an isotope of carbon and is the basic component of graphite. Graphene has been widely used in electronics and optics [26,27], mainly because of its ultrafast relaxation time (relaxation time <200 fs), low saturation energy, and large modulation depth. In addition, graphene is a zero-energy-gap semiconductor with excellent nonlinear optical properties that allow it to produce a broadband nonlinear response in the visible to IR optical band. In 2013, a mode-locked laser at 2 μm with multilayer graphene was completed by Sobon [28]. They have experimentally demonstrated for the first time that graphene has good SA properties in the mid-IR band.

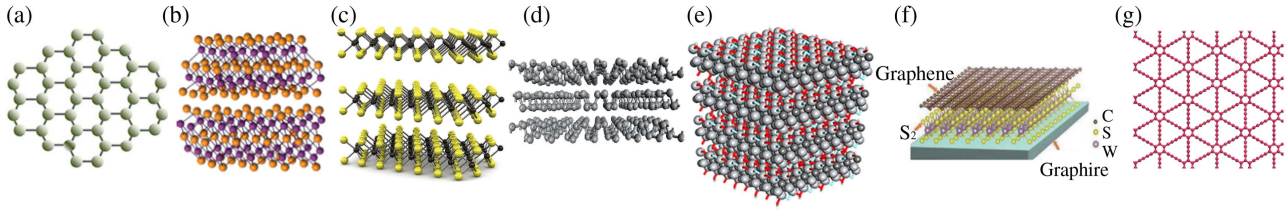

Fig. 2. Atomic structures of 2D materials. (a) Graphene; (b) TIs; (c) TMDs; (d) BP; (e) MXenes; (f) heterostructures; (g) graphdiyne; (a) Reprinted from Ref. [19], copyright 2020, IEEE; (b) reprinted from Ref. [20], copyright 2012, American Chemical Society; (c) reprinted from Ref. [21], copyright 2019, AIP Publishing; (d) reprinted from Ref. [22], copyright 2012, Wiley; (e) reprinted from Ref. [23], copyright 2021, De Gruyter; (f) reprinted from Ref. [24], copyright 2017, Chinese Laser Press; (g) reprinted from Ref. [25], copyright 2016, Springer Nature.

TIs are a new Dirac material with an asymmetric topological order. The surface is in the gapless conducting state, but the bulk state is an insulator, and the band gap of TIs can be adjusted by varying the material thickness and making heterostructures. Their atomic structure is shown in Fig. 2(b) [20]. Generally, TIs include Sb_2Te_3, Bi_2Se_3, and Bi_2Te_3 with a band gap of 0.2–0.3 eV [29–32]. TIs have broadband absorption properties and can be used as SAs in pulsed lasers. In 2012, Bi_2Te_3 was first used as an SA in ultrafast lasers [33]. Since then, other TI materials have been widely reported in *Q*-switched lasers and mode-locked lasers.

TMDs are a class of semiconductor materials with the chemical formula MX_2, where M is a transition metal element (such as Mo, W, and Ti) and X is a sulfur group element (such as S, Se, and Te). The structure of TMDs is similar to a sandwich, which consists of two layers of X elements sandwiching a layer of M elements, the atoms within the layers are combined with covalent bonds, and the layers are combined with van der Waals forces. So far, the common TMDs reported are MoS_2, WS_2, $MoSe_2$, WSe_2, $MoTe_2$, and WTe_2. Figure 2(c) shows the atomic structure of MX_2 [21]. These materials are semiconductors with an indirect band gap in bulk form. However, when the layers are thinned to monolayers, they exhibit an indirect band gap to direct band-gap transition, mainly due to the progressive enhancement of quantum confinement, which ranges from 1.0 to 2.0 eV for different TMDs materials [34–37]. Thus, the photoluminescence in monolayer TMDs is several orders of magnitude stronger than that in their bulk materials, even if the amount of materials in monolayer TMDs is much smaller. Numerous experimental results have demonstrated that the band gap of TMDs can be adjusted by controlling the number of layers of materials, a property that broadens the scope of TMDs in electronics applications [38–40].

BP, which is an isomer of phosphorus, is a layered direct band-gap semiconductor first synthesized in the 1960s [41]. It is a honeycomb-like layered crystalline material formed by the folding of a single BP layer, and the number of layers can vary from a single layer to several layers. This property allows the band gap of BP to fill the gap between graphene and TMDs because its band gap can be tuned from 0.3 eV for bulk to 2.0 eV for a single layer by changing the number of layers [42]. BP is widely used as an SA to make a variety of functional optical devices due to its high carrier mobility, controllable forbidden bandwidth properties, and unique in-plane anisotropic structure [42–45]. Figure 2(d) shows the atomic structure of BP [22]. In 2015, a mode-locked *Q*-switched fiber laser with BP as an SA at the wavelength of 1550 nm was first reported [46].

Transition metal carbides and nitrides, a 2D material family widely known as MXenes, have unique properties that can be altered by simply controlling the composition and surface terminating elements [47]. MXenes have the general form $M_{n+1}X_nT_x$, where M denotes a transition metal (such as Ti, Ta, Cr, or Mo), X denotes C and/or N, T is a surface termination (O, OH, or F), and $n = 1$, 2, or 3. The corresponding atomic structure is given in Fig. 2(e) [23]. Due to its high elastic modulus, tunable band gap, good electrical conductivity, high optical transparency, and good stability at room and ambient temperatures, it has attracted much attention in different research fields, and the typical $Ti_3C_2T_x$ has been extensively studied. Studies have shown that the effective nonlinear absorption coefficient of $Ti_3C_2T_x$ ($\beta_{eff} \sim -0.297$ cm/GW) is slightly lower than that of graphene oxide (~ -2.2 cm/GW), which is lower than that of MoS_2 (~ -0.004 cm/GW) and BP (~ -0.006 cm/GW) by two orders of magnitude, suggesting that $Ti_3C_2T_x$ should have a strong optical switching capability [16,48–51]. In addition, $Ti_3C_2T_x$ has a high damage threshold 70 mJ/cm^2 compared to other 2D materials [52], which is a key parameter for excellent SAs.

Layered material heterostructures are structures assembled by stacking materials with different optical properties on top of each other that consist of strong in-plane covalent bonds and out-of-plane weak van der Waals interlayer forces [53]. Great effort has been put into exploring different heterostructures, including, but not limited to, graphene–hexagonal boron nitride (hBN), graphene–BP, TMD–hBN, TMD–graphene, and TMD–TMD combinations [54]. Figure 2(f) shows the atomic structure of the graphene–Bi_2Te_3 heterostructures prepared by Zhang using the secondary chemical vapor deposition (CVD) growth method [24]. In the heterostructures dominated by van der Waals forces, the materials can maintain their respective optical properties while achieving electron migration and interband leap through interlayer coupling, thus achieving optical synergy [55,56]. Optoelectronic devices made from composite materials have better optical response performance and optical response time [57,58], which will lead to higher quality mode-locked signals. Therefore, compared to a single 2D material, a heterostructure composed of more than two types of 2D materials has better future as a new nonlinear optical material. Heterostructures composed of two or more

2D materials will lead to more exciting discoveries as new nonlinear optical materials compared to single 2D materials.

It is well known that graphene and similar derivatives are making a splash in fiber-locked lasers, but here it is important to highlight a very important class of materials in its family, namely, graphdiyne (GDY). In 1997, Haley *et al.* proposed a class of graphdiyne consisting of a diacetylene group and benzene ring in the graphene family [59]. Then, in 2010, the Institute of Chemistry of the Chinese Academy of Sciences successfully synthesized a large area (3.61 cm^2) of graphdiyne films on the surface of copper sheets by using a coupling reaction of hexaethynylbenzene under the catalytic effect of copper sheets [60]. Since then, graphdiyne has been transferred from the theoretical structure to the experimental platform. Compared to graphene, which is derived from sp^2 hybridization, graphdiyne is a composite of sp and sp^2 hybridization, producing a high π conjugated structure with two acetylene bonds between benzene rings. The atomic structure of graphdiyne is shown in Fig. 2(g) [25]. It has the advantages of abundant carbon chemical bonding, a large conjugation system, more active sites, excellent chemical stability, and controlled heteroatom doping [61–63]. It is its special electronic structure and natural pore structure that offer important potential applications in electrochemistry, catalysis, environment, energy, and other fields [64–68]. As a result of all the in-depth research being done on GDY, it is beginning to emerge as a nonlinear material in the field of ultrafast lasers. By density functional theory calculations, some light metals can be adsorbed on the GDY structure based on the complete relaxation of the GDY geometry as LM1-3 at GDY (LM = Li, Na, Ca, and Ti). This structure has an intramolecular electron donor–acceptor framework and exhibits uncommon nonlinear optical properties. And, unlike graphene, which has a zero band gap, GDY has a natural band gap that can be regulated between 0.46 and 1.22 eV by varying the hydrogen coverage [63]. Therefore, it has excellent application properties in near-IR optics. Guo *et al.* first investigated and demonstrated the broadband saturable absorption and transient absorption properties of GDY from the visible to the IR in 2020 [69]. This accomplishment showed that GDY has stronger nonlinear absorption, lower saturation intensity, and ultrafast relaxation time compared to conventional 2D materials. As a result, GDY can be used as a new type of 2D material for a wide range of photonics devices.

B. Fabrication Strategies and Characterization of 2D Materials

After browsing and studying a large amount of literature, one conclusion can be drawn: high-quality material samples are the key to good experimental data in later experiments. In recent years, there are several strategies to prepare 2D materials from chemical and physical perspectives, which can be generally summarized as top-down exfoliation, bottom-up growth [70], and topological transformation methods [71]. A macro overview of top-down and bottom-up manufacturing methods is shown in Fig. 3.

Top-down exfoliation is a means to prepare single-layer or few-layer 2D materials through the weaker van der Waals force between the layers of 2D materials, including mechanical exfoliation (ME) [76], liquid-phase exfoliation (LPE) [77,78],

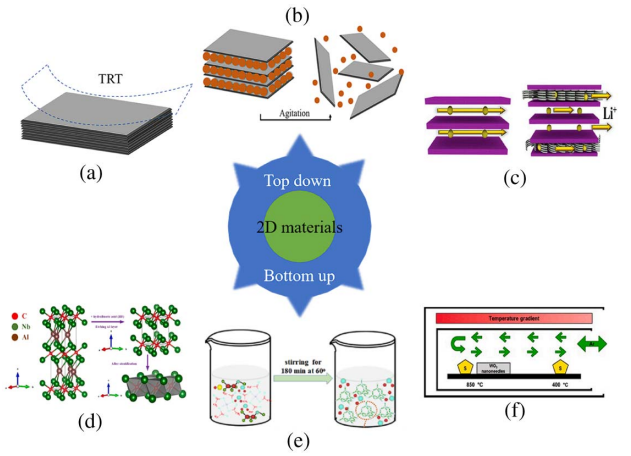

Fig. 3. Overview of bottom-up and top-down approaches to 2D materials fabrication. (a) ME; (b) LPE; (c) ion embedding and stripping; (d) aqueous acid etching; (e) magnetron-sputtering deposition; (f) CVD. (c) Reprinted from Ref. [72], copyright 2020, Elsevier; (d) reprinted from Ref. [73], copyright 2021, Elsevier; (e) reprinted from Ref. [74], copyright 2021, American Chemical Society; (f) reprinted from Ref. [75], copyright 2021, Elsevier.

and ion-intercalation peeling. Bottom-up growth is used to form 2D materials at the molecular level by chemical means, specifically including CVD [79], the magnetron-sputtering deposition method, and aqueous acid etching. These widely used methods for the preparation of 2D nanomaterials (ME, LPE, and CVD) will all be discussed in more depth below.

ME, also known as the "transparent tape method," is a simple, inexpensive method to repeatedly exfoliate bulk materials with tape to obtain a single layer or a few layers of 2D materials. This method has been used in basic research to produce nanomaterials with high crystallinity, few defects, structural integrity, and clean surfaces. Its shortcomings are evident in the extremely low yield and uncontrollability, so it is only suitable for small-scale laboratory preparation. LPE is a physical method that uses ultrasound-generated bubbles to continuously disrupt the van der Waals forces between layers and then removes the unexfoliated nanomaterials by centrifugation [80]. It is an effective, feasible method with a low cost, which can offer high yields of mixed and composite layered materials. However, the same disadvantages exist: the yield of single-layer, large-sized nanomaterials is relatively low, and the size of the materials is difficult to control. The CVD method is a chemical reaction in the gaseous or powder state to produce a solid material deposited on the surface of a substrate, resulting in the synthesis of high-quality 2D materials. Compared to LPE and ME, this important process technology can be controlled by adjusting the reaction parameters to regulate the number of layers during the material preparation process, and the quality, yield, and size can be guaranteed to a certain extent [81]. However, the substrate material suitable for its ideal condition is expensive, and the equipment and process involved are relatively complex. As a result, this preparation method has a high cost, which makes it most suitable for large-scale commercial production.

It is well known that the properties of a material depend to a large extent on its structure. Each step of material production leaves traces in the material organization in the form of hole shape and volume, inclusions orientation, and size. Therefore, quantitative structural characterization is essential to assess the properties of materials and their performances in practical applications. For 2D nanomaterials, we characterize them by various techniques such as SEM, atomic force microscopy (AFM), transmission electron microscopy (TEM), higher resolution transmission electron microscopy (HRTEM), and Raman scattering spectroscopy (Raman). SEM offers high resolution, wide magnification, good image depth of field, simple sample preparation, and comprehensive analysis capability. SEM is due to the interaction of the focused electron beam with the sample and various signals generated to excite a variety of images of information. In SEM at any moment the electron beam and a point on the sample interact; when scanning point by point, the intensity of the signal is changing, which reflects the difference between the points on the sample. AFM is a high-resolution detection technique based on the interaction forces between atoms to study the surface structure and properties of materials. It uses the tip of a needle on a microcantilever in contact with the surface, and the isotope of interatomic forces on the sample surface while undulating motion in the direction perpendicular to the surface of the sample, using the repulsive forces between atoms to restore the appearance of the atoms. Hence, AFM can be used to characterize important properties such as the appearance and nanomechanics of materials. TEM is a technique that uses a shorter wavelength electron beam (instead of visible light) that diffracts to obtain a 2D image; therefore, the surface image is seen along with the inner material. This is a very important tool for the microscopic characterization of 2D materials, allowing the observation of curved material edges or folded stripes in the sample without external influences to determine the number of layers of material with high accuracy; HRTEM has a higher resolution than TEM, can see more microscopic material, can directly probe the structure of crystals, and can also be used to observe the phase lining image of very thin specimens, with a thick scale resolution capability. Raman can be used to determine the number of layers and quality of a sample quickly and accurately by characterizing the peak intensity, peak area, peak shift, and full-width at half maximum in the Raman spectrum. It can also be used to investigate changes in the electronic structure of a material. Characterization images of 2D materials fabricated based on ME, LPE, and CVD will be presented in Fig. 4 [82–84]. For the ME method and CVD method, AFM, SEM, and Raman are mainly applied to characterize the materials as shown in Figs. 4(a)–4(c) and 4(d)–4(f). Among them, AFM and SEM are mainly used to confirm the thickness and uniformity of the materials to determine whether the height difference of the material surface is within the acceptable range. Raman spectroscopy is used to measure the Raman shift of the materials. As for the material prepared by the LPE method, which is shown in Figs. 4(d)–4(f), not only must the thickness of the material be determined by applying AFM, but TEM and HRTEM also are needed to show, respectively, the thin properties of each nanomaterials layer and the highly crystalline nature of the nanosheets.

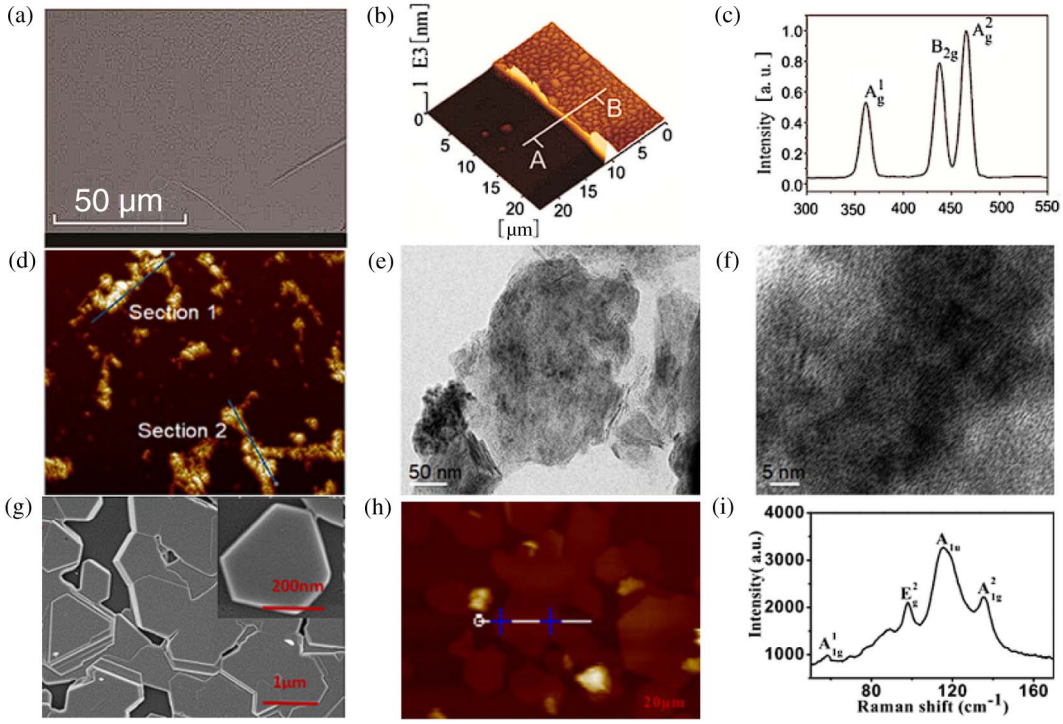

Fig. 4. Structural characterization of 2D materials based on diverse preparation methods. (a)–(c) SEM, AFM, and Raman images of BP based on ME; (d)–(f) AFM, TEM, and HRTEM images of V_2CT_x based on LPE; (g)–(i) SEM, AFM, and Raman images of Bi_2Te_3 based on CVD. (a)–(c) Reprinted from Ref. [82], copyright 2016, Optica; (d)–(f) reprinted from Ref. [83], copyright 2022, Elsevier; (g)–(i) reprinted from Ref. [84], copyright 2019, Optica.

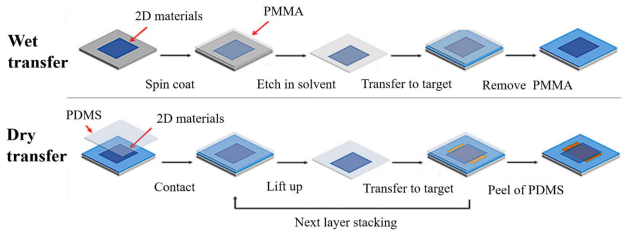

Fig. 5. Two main transfer techniques for 2D materials. Reprinted from Ref. [85], copyright 2019, Wiley.

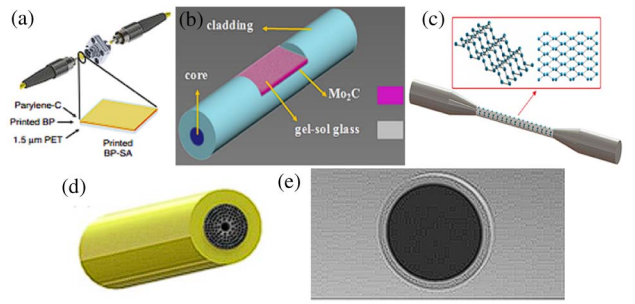

Fig. 6. Integration of SAs based on 2D materials: (a)–(d) fiber laser devices, (e) solid-state laser device. (a) Sandwiching structure transferring SA on fiber end; (b) D-shaped fiber; (c) tapered fiber; (d) photonic crystal fiber; and (e) free-space coupled substrates. (a) Reprinted from Ref. [86], copyright 2017, Springer Nature; (b) reprinted from Ref. [74], copyright 2021, American Chemical Society; (c) reprinted from Ref. [87], copyright 2018, IOP Publishing.

C. Integration Strategies Based on 2D Nanomaterial SAs

2D materials as SAs cannot act directly in lasers because the thin sheets of 2D materials are approximately nanometers thick. Therefore, they must be subjected to a special coupling design to facilitate the interaction of light with 2D materials. For solid-state lasers, SAs must have high damage thresholds, while increasing the area to reduce the energy density. As shown in Fig. 5, there are two main transfer techniques: wet transfer and dry transfer [85]. The wet transfer method, which is widely used for 2D materials fabricated by CVD and ME, has three steps: first, the 2D material dispersion is mixed with an organic reactive material such as polymethyl methacrylate (PMMA); next, 2D materials polymer film is transferred to the substrate through a spin-coating process; and finally, the polymer-coated sample is separated from the substrate. The wet transfer method is an easy processing method, but residual polymer, as well as irregular folds and cracks, is difficult to avoid, and excessive cleaning steps contribute to the tedious nature of the preparation. The dry transfer method can compensate for the disadvantages of the wet transfer approach to some extent. First, the 2D materials are peeled off from the substrate by multiple imprinters [dimethyl siloxane, polydimethylsiloxane (PDMS)]; then, an impression is brought into contact with another to lift the 2D layer on the impression; and third, the process above is repeated to obtain more 2D layer stacks with clean interfaces.

The devices based on 2D material integration strategies in solid-state lasers and in fiber lasers are shown in Fig. 6. Due to the customizability of the fiber morphology, the integration strategies for fiber laser devices are far more than those for solid-state lasers. For fiber lasers, the 2D materials coupled to the cavity can be divided into two categories: the transmission integration method and the swift wave integration method. The transmission integration method is a sandwich structure formed by inserting a small piece of material directly into the two fiber ends, as shown in Fig. 6(a) [86]. The transmission integration method is suitable for thin-film 2D nanomaterial devices, with the advantage of a simple structure. There is, however, a disadvantage: the close connection of two fiber ends leads to heat accumulation at the exit end and a low damage threshold of the device. The swift wave integration method usually refers to the interaction between the material and the light through the swift field and the final adsorption on the surface of the acting fiber. For example, the photodeposition of D-shaped fibers [Fig. 6(b)] [74] and tapered fibers [Fig. 6(c)] [87] is used to obtain mode-locked laser pulses by wrapping the D-shaped fiber or tapered fiber with the material. For the integration method of tapered fiber and 2D materials, optical deposition is often used. As in Ref. [88], the tapered fiber is connected to the pump light, the material is dropped on the finest part of the tapered area, and the material is adsorbed onto the fiber surface based on the coupling between the tapered fiber surface evanescent field and the 2D materials, and the deposition process is observed using microscopy. The advantage of the swift wave integration method for solution-based 2D nanosheets is that the nonlinearity and damage threshold of a device are increased due to the longer light–matter interaction distance, but the disadvantage is that it is difficult to precisely regulate the 2D material distribution during the photodeposition and the device reliability is poor. A structure combining nanomaterials and photonic crystal fiber is depicted in Fig. 6(d), which also has the advantage of a high damage threshold and strong nonlinearity, but its coupling efficiency is low. When 2D nanomaterial SAs are used in solid-state lasers, the structures depicted in Fig. 6(e) are usually used, where 2D nanomaterials are deposited onto substrates such as YAG, quartz, or a gold mirror. The interaction of materials with light in this structure is achieved by transmission or reflection of spatial optical coupling.

D. Nonlinear Optical Properties Testing of 2D Materials

2D materials are currently used as SAs to generate ultrafast pulsed lasers, which are achieved by exploiting the saturable absorption properties of the materials and have been extensively reported. In particular, there are three important parameters to characterize the saturable absorption properties of materials: the modulation depth (α_s), the saturation intensity (I_{sat}), and the unsaturated loss (α_{ns}). The relationship between the nonlinear transmittance (T) and the incident light intensity (I) and the relationship between the absorption coefficient (α) and the incident light intensity (I), can be expressed by

$$T(I) = 1 - \Delta T \times \exp(-I/I_{sat}) - T_{ns}, \quad (1)$$

$$\alpha(I) = \alpha_{ns} + \frac{\alpha_s}{1 + I/I_{sat}}, \quad (2)$$

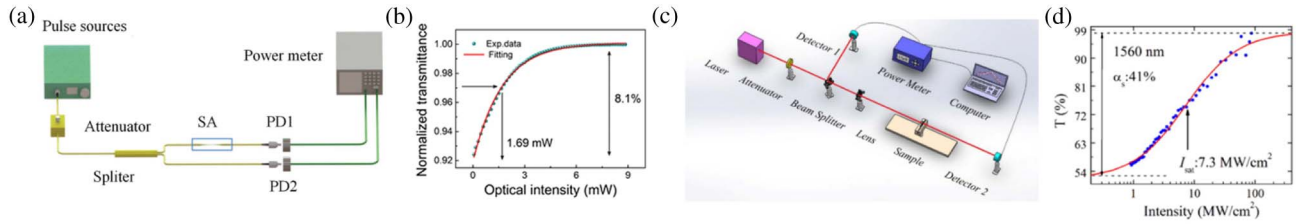

Fig. 7. Nonlinear optical properties test method. (a) Setup of the I-scan technique measurement. (b) Saturable absorption property of the PQD SAs device. (c) Schematic diagram of the experimental setup for Z-scan measurement. (d) Relationship between Z-scan nonlinear transmittance and incident light energy intensity. (a), (b) Reprinted from Ref. [91], copyright 2017, Springer Nature; (c), (d) reprinted from Ref. [92], copyright 2019, Chinese Laser Press.

where $T(I)$ is the transmittance, ΔT is the modulation depth, and T_{ns} is the nonlinear loss.

Two main methods are used to measure the nonlinear optical properties of 2D materials: the open-aperture I-scan (known as the balanced twin-detector technique) method [89] and the Z-scan measurement method [90]. The I-scan technique is presented in Fig. 7(a), where an ultrashort pulse light source is used as the excitation light source, and a 50:50 damped coupler is used to split it into two beams, the reference data detector (detector PD1) and the absorption detector (detector PD2). The nonlinear saturation absorption characteristic curve of the material is obtained by fitting the experimentally obtained transmittance to the equation above [Fig. 7(b)] [91]. This method is limited in testing nonlinear saturable absorption properties with high optical power dependence because the optical transmission is confined inside the fiber, but it is still considered one of the best choices for nonlinear saturable absorption properties of 2D nanomaterials due to its compactness and operational simplicity. The Z-scan technique setup is illustrated in Fig. 7(c). During the measurement, the sample is scanned longitudinally with the focal plane of the focused Gaussian beam as the detection source. The intensity distribution of the transmitted light received by the detector through the finite aperture diaphragm at the far-field varies with the position of the sample, which is called a closed-aperture Z-scan because of the diaphragm in front of the detection light. The transmission intensity usually is measured directly by removing the diaphragm for the open-aperture Z-scan, and the normalized transmission intensity is obtained. A typical graph of the saturable absorption properties based on a Z-scan is shown in Fig. 7(d) [92]. Table 1 compares the two inspection methods for 2D materials, I-scan and Z-scan, and summarizes their saturation intensity and modulation depth.

3. MODE-LOCKED LASERS AT 1.5 AND 2 μm WITH 2D MATERIALS AS SAS

Solid-state lasers and fiber lasers are the two most dominant types of lasers that can obtain ultrafast lasers. Figure 8 illustrates the typical cavity structure of both lasers. Solid-state lasers are widely used in microfabrication fields, which can convert IR light into green light, UV light, and other wavelength beams by nonlinear crystal frequency doubling, with good beam quality, high single-pulse energy, high output peak power, and low thermal effect. However, its large size and susceptibility to interference from external vibration and temperature changes limit the large-scale commercial application of solid-state lasers, and it is relatively difficult to achieve mode-locked solid-state lasers. Fiber lasers are often used for ultrafast laser precision processing, and their gain medium requires only the addition of rare earth elements in the fiber to form an activation medium, which is inexpensive and small compared to solid-state lasers. In addition, fiber lasers also have the advantages of a wide output wavelength range and stable performance and are less susceptible to external interference; however, due to the small diameter of the fiber core, the peak power it can withstand is not too high and the single pulse energy is low. Solid-state lasers and fiber lasers have their advantages and disadvantages according to different application fields and different performance parameters. We mainly introduce and

Table 1. Comparison of the Data Obtained for the Two Inspection Methods for 2D Materials

	I-scan			Z-scan		
2D Materials	I_{sat} /(MW cm^{-2})	ΔT/%	Ref.	I_{sat} /(MW cm^{-2})	α_s/%	Ref.
Graphene	60.00	3.90	[93]	0.87	17.40	[17]
Bi_2Se_3	90.20	39.80	[94]	490.00	98.00	[95]
Bi_2Te_3	28.00	6.20	[96]	480.00	95.30	[33]
MoS_2	85.40	25.30	[97]	413 ± 24 GW cm^{-2}	34.40	[98]
WSe_2	15.42	21.89	[99]	7.00	5.4	[100]
WS_2	19.80	35.10	[101]	156 GW cm^{-2}	35.75	[102]
BP	8.30	10.00	[87]	14.98	10.03	[103]
$Ti_3C_2T_x$	256.90	0.96	[104]	7.30	41.00	[92]
V_2CT_x	0.5 mW cm^{-2}	48.80	[105]	100.02	20.20	[83]
Graphdiyne	48.00	21.10	[106]	4.03	48.13	[107]

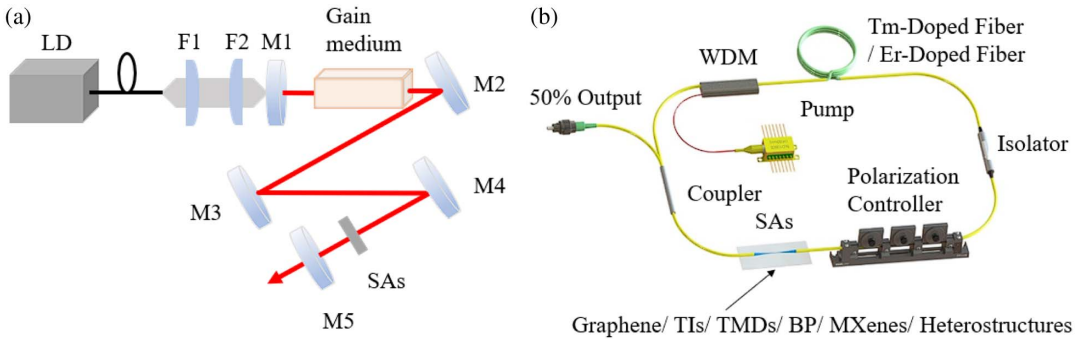

Fig. 8. Typical cavity construction: (a) solid-state lasers and (b) fiber lasers.

analyze the ways to realize ultrashort pulses based on 2D material integrated devices and their output performances.

A. Solid-State Mode-Locked Lasers Based on 2D Materials

Solid-state lasers have a longer development history compared to fiber lasers. In 1960, Theodore Maiman invented the ruby laser at the Hughes Research Laboratories in California, which is the world's first solid-state laser. Since then, the composition of solid-state lasers has been continually improved, and the cavities of common solid-state lasers are now mainly composed of reflecting mirrors and solid-state gain media and equipped with pump sources and SAs and other important devices to constitute the prototypes of solid-state lasers. Previously, SESAM-based, nanomaterial-based solid-state mode-locked lasers were reported. In recent years, with the continuous research and discovery of 2D materials, the development of solid-state lasers has been boosted once again. At present, solid-state, mode-locked lasers based on 2D materials are mainly concentrated around 1 μm and are quite well developed. Therefore, the main parameters and properties of solid-state, mode-locked lasers in the 1.5 μm and 2 μm bands have been summarized in this review. The commonly used gain media at 1.5 μm are Nd:$GdVo_4$, Nd:YVO_4, Cr:YAG, and so on, and the commonly used gain media at 2 μm are Tm:CLNGG, Tm:YAP, Tm:YAG, Tm:CYA, Tm:LLF, Tm, Ho:$LiYF_4$, Tm:LuAG, Tm:Lu_2O_3, and Tm, Ho:LLF. Note that the difference in gain media has a slight influence on the nature of solid-state lasers, which can obtain different wavelengths of mode-locked lasers.

Table 2 summarizes the performance of solid-state, mode-locked lasers based on graphene, TMDs, and BP 2D materials. Note that at the wavelengths 1.5–2 μm, solid-state mode-locked lasers based on 2D materials are mainly based on graphene and TMDs as SAs, and the solid-state, mode-locked lasers based on other 2D materials are less reported. Also note that most of the reported lasers are passively *Q*-switched. This phenomenon is related to the fact that mode-locked lasers are difficult to form. Solid-state lasers often require refraction of the optical path to obtain ps-level or even fs-level mode-locked lasers, which often results in large errors and uncertainties in the data obtained. On the other hand, this phenomenon may be related to the material preparation. As mentioned above, the large size, good homogeneity, and a controllable number of layers of graphene and TMDs prepared by CVD are important advantages to obtain excellent solid mode-locked

Table 2. Performance Summary of Mode-Locked Solid-State Lasers Based on Graphene, TMDs, and BP at 1.5–2 μm

SA		Gain Medium	λ/nm	Pulse Width/ps	Repetition Rate/MHz	Peak Power/kW	Ref.
Graphene		Nd:$GdVO_4$	1341.10	11.000	100.00	1.173	[108]
		Nd:YVO_4	1342.40	7.400	44.60	0.667	[109]
		Cr:YAG	1516.00	0.091	85.16	12.904	[110]
		Tm:CLNGG	2014.40	0.882	95.00	0.716	[111]
		Tm:CLNGG	2018.00	0.729	99.00	0.834	[112]
	G-Gold	Tm:CLNGG	2010.00	0.354	98.00	2.796	[113]
	GO	Tm:YAP	2023.00	<10	71.80	0.373	[114]
		Tm:YAP	1988.00	–	62.38	–	[115]
		Tm, Ho:LiF_4	2051.00	5.800	69.80	0.198	[116]
	GO	Tm:LuAG	2023.00	923.800	104.20	0.018	[117]
		Tm:Lu_2O_3	2067.00	0.410	110.00	5.987	[118]
TMDs	MoS_2	Nd:YVO_4	1342.50	0.8 μs	98 kHz	7.653 W	[119]
	TiS_2	Tm:YAG	2011.40	224.000	208.50	2.184 W	[120]
	WS_2	Tm, Ho:LLF	1895.00	878.000	131.60	0.001	[121]
	MoS_2	Tm:YAG	2011.00	280.000	232.20	0.003	[122]
	MoS_2	Tm:CYA	1863.00	994.000	103.70	0.011	[123]
	MoS_2	Tm:LLF	1918.00	–	83.30	–	[124]
	MoS_2	Tm:YAP	1932.00	100.000	92.10	0.012	[125]
BP		Nd:$GdVO_4$	1340.50	9.240	58.14	7.369	[126]

data. In addition to CVD, LPE is also a common means of laboratory preparation in the field of solid-state lasers, where 2D materials with a small number of layers and a large size can be obtained by ultrasound, centrifugation, and other auxiliary methods.

In 2010, researchers obtained mode-locked pulses in a solid-state laser based on graphene as the SA with a gain medium of Nd:YAG [17]. This work has greatly contributed to the application of graphene and other layered materials in mode-locked solid-state lasers. At present, mode-locked laser technology for solid-state lasers based on 2D materials at wavelengths near 1 μm is quite mature. In 2018, Tao *et al.* used layered $PtSe_2$ (TMDs) as SAs for the first time to generate ultrafast mode-locked laser pulses. A peak output power of 185.8 W was obtained at a central wavelength of 1066.6 nm with a pulse width of 15.8 ps and a repetition frequency of 61.3 MHz [127]. This report can especially highlight the promising applications of 2D materials at 1 μm. For the mid-IR of 3 μm, it is relatively difficult to realize and build solid-state mode-locked lasers due to the strong absorption of water in this region and the special energy level structure of the gain medium, and few reports are available on this topic. In 2019, researchers obtained ps pulses for the first time from a graphene-based solid-state laser of Nd:YVO_4 at a wavelength of 1.34 μm [109], as depicted in Figs. 9(a)–9(c). In this work, they proposed the insertion of a $\lambda/8$ thick SiO_2 layer and a $\lambda/4$ thick SiO_2 layer between a monolayer of graphene and an HR mirror. Using this approach, they could compare the performance in terms of the generation of ultrafast lasers. The GSAM with $\lambda/8$ SiO_2 film is more suitable for high-power mode-locked lasers or low emission cross-section gain media (e.g., ytterbium-doped crystals), while the GSAM with $\lambda/4$ SiO_2 film is more suitable for short pulse generation with a wide spectral width. This proposed method made a great contribution to the flexible tuning of saturable absorption properties of other 2D nanomaterials in the future. In 2017, Sun *et al.* completed the first BP-based mode-locked solid-state laser in the 1.34 μm spectral region [126]. As shown in Figs. 9(d)–9(f), they fabricated ~7-layer BP nanosheets as an SA using LPE with a band gap calculated at 0.62 eV. After that, nonlinear optical tests were performed on the BP material. The results showed that the modulation depth and saturation flux were determined to be 16% and 1.3 $\mu J/cm^2$, respectively, and the nonsaturation loss of the BP SA was estimated to be 8.35%. The solid-state mode-locked laser had a maximum peak power of 7.37 kW and a repetition frequency of 58.14 MHz. A mode-locked pulse with a duration of 9.24 ps was obtained at a wavelength of 1340.5 nm. As shown in Table 2, the realization of solid-state laser mode-locking at 2 μm is more reported relative to the realization of solid-state laser mode-locking near 1.5 μm because the gain medium in the 2 μm region is more doped with rare metals. As early as 2012, researchers made a solid-state mode-locked laser with Tm:YAP as the gain medium based on graphene oxide as an SA [114], and the pulse width reached a sub-10 ps path. In

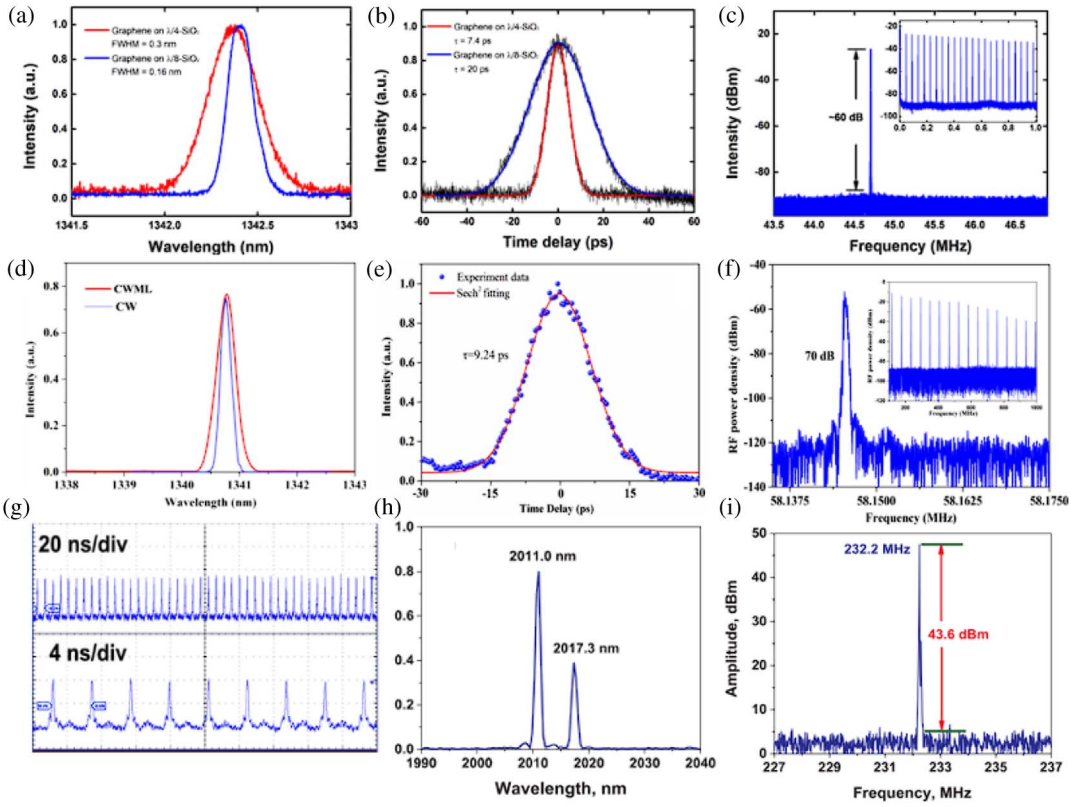

Fig. 9. Mode-locked solid-state laser based on 2D layered nanomaterials. (a), (d), and (h) Corresponding output spectrum. (b) and (e) Normalized autocorrelation trace. (c), (f), and (i) Radio spectrum. (g) Oscilloscope traces of typical QML pulse trains at different time scales. (a)–(c) Reprinted from Ref. [109], copyright 2019, IEEE; (d)–(f) reprinted from Ref. [126], copyright 2017, Optica; (g)–(i) reprinted from Ref. [122], copyright 2020, Elsevier.

2020, Li *et al.* demonstrated for the first time the passively mode-locked operation of a Tm:YAG laser with MoS_2 SAs [122]. As shown in Figs. 9(g)–9(i), they employed the use of an ultrasonic thermolysis method to synthesize a MoS_2 solution and spin-coated it on the mirror surface. By performing nonlinear optical tests on this SA, the saturated absorption intensity, modulation depth, and raw transmittance can be calculated as 37.94 mJ/cm^2, 2.9%, and 89.2%, respectively. The experimental optical path was studied by building a z-fold cavity for a passive *Q*-switched mode-locked Tm:YAG laser. It is conceivable that a higher output performance can be theoretically obtained by further optimizing the structure of the resonant cavity; for example, if an X-shaped resonant cavity is used or the length of the resonant cavity is increased by increasing the number of reflectors. The results of this experimental success show that a minimum pulse width of 280 ps and a pulse repetition rate of 232.2 MHz can be obtained at 2011 nm. In addition, it corresponds to a calculated pulse energy of 0.86 nJ and a peak power of 3.07 W. In fact, Ma *et al.* achieved an ultrashort pulsed laser using a graphene SESAM that could obtain a pulse width of 32 fs [128]. This is the shortest pulse width that can be obtained from a solid-state mode-locked laser based on 2D materials. Its central wavelength is 1068 nm, and its repetition frequency and maximum average output power are 113.5 MHz and 26.2 mW, respectively. Zhao *et al.* earlier had prepared a molybdenum sulfide and graphene oxide composite and built a V-shaped resonant cavity to achieve a mode-locked laser with a repetition frequency of up to 1 GHz, which is the largest repetition frequency available [129].

B. Fiber Mode-Locked Lasers Based on 2D Materials

Tables 3 and 4 summarize the pulse characteristics of mode-locked fiber lasers based on 2D materials at wavelengths of 1.5 μm and 2 μm, respectively. Note that the wavelength range of fiber lasers is still mainly focused on 1.5 μm, and relatively little research has been done on 2 μm, which may be related to the development of optical fiber. The development of 1 μm mode-locked fiber laser is relatively mature and has achieved outstanding success, while the cost of 2 μm region fibers is higher. In addition, current optical fibers have large losses for 3 μm. From Table 2, we can see that the pulse width of mode-locked fiber lasers based on 2D materials is mainly concentrated at 0–2 ps, and the repetition frequency is mainly concentrated at 0–100 MHz. Currently, the shortest pulse width of ultrafast lasers based on 2D materials is 29 fs, which is the ultrafast pulsed laser with an output power of ~52 mW and pulse energy of 2.8 nJ achieved in 2015 by Purdie *et al.* by using a graphene SA [215]. The maximum repetition frequency of ultrafast lasers based on 2D materials is 3.27 GHz (212th harmonic), which was achieved by Koo *et al.* in 2016 using $MoSe_2$/PVA SAs, and the autocorrelation curve corresponding to a single pulse with a pulse width of 798 fs [216]. In addition, Liu *et al.* achieved a maximum pulse energy of 325.50 nJ and a maximum available

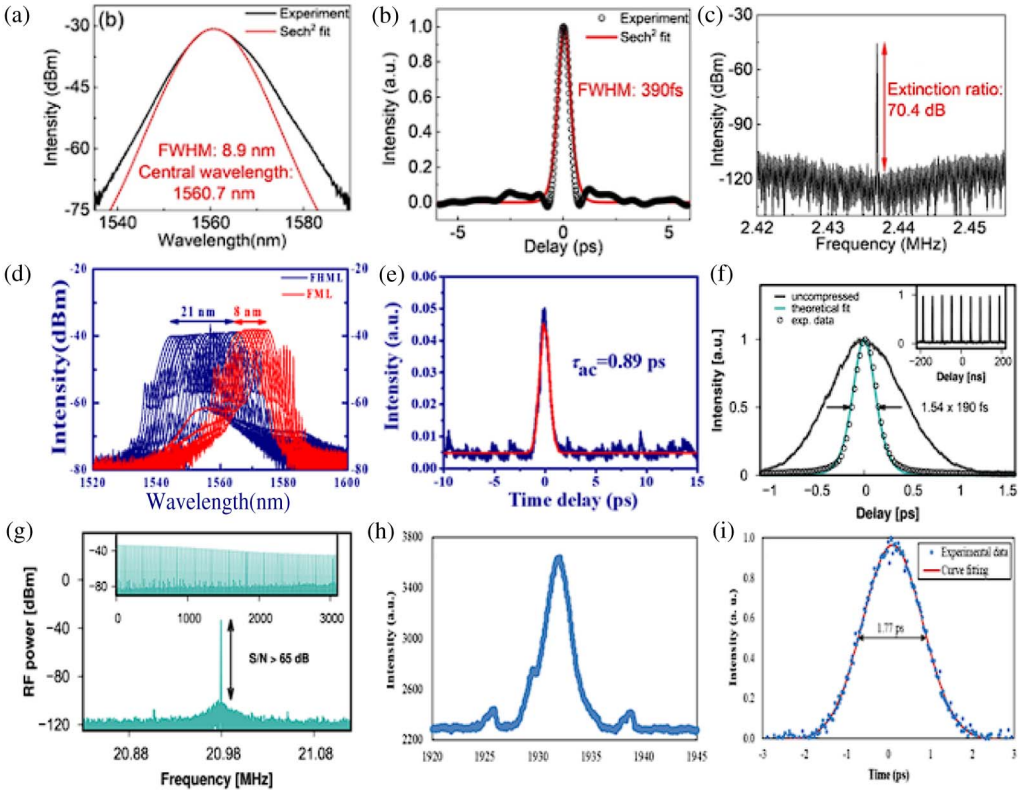

Fig. 10. Graphene mode-locked fiber laser at wavelengths of 1.5 μm and 2 μm. (a), (d), and (h) Optical spectra. (b), (e), (f), and (i) AC traces of mode-locked pulses. (c) and (g) Repetition frequency. (a)–(c) Reprinted from Ref. [133], copyright 2020, American Chemical Society; (d), (e) reprinted from Ref. [135], copyright 2021, Elsevier; (f), (g) reprinted from Ref. [193], copyright 2018, Optica; (h), (i) reprinted from Ref. [197], copyright 2021, Elseriver.

Table 3. Performance Summary of Mode-Locked Fiber Lasers Based on 2D Layered Materials at 1.5 μm

SA		Integration	λ/nm	Pulse Width/ps	Repetition Rate/MHz	Peak Power/W	Ref.
Graphene		Sandwich	1576.30	0.415	6.84	17,590.36	[130]
		Sandwich	1564.00	0.870	19.30	11.95	[131]
	GO	Sandwich	1559.56	0.582	23.21	1301.43	[132]
		D-shaped	1560.70	0.390	2.44	–	[133]
		Sandwich	1557.78	7.820	1.65	1062.66	[134]
	GO	Tapered	1599.43	0.568	5.68	2095.07	[93]
	GO	Sandwich	1574.00	0.890	–	–	[135]
TIs	Bi_2Te_3	D-shaped	1547.32	0.600	15.11	–	[136]
	n Bi_2Te_3	SMF	1570.00	0.400	–	–	[137]
	p Bi_2Te_3	SMF	1543.45	0.385	–	–	[137]
	Bi_2Te_3	Tapered	1562.40	0.320	17.34	100.92	[96]
	Bi_2Te_3	D-shaped	1559.40	266.000	5.50	1.30	[138]
	Bi_2Te_3	Sandwich	1570.45	0.505	13.14	–	[139]
	Bi_2Te_3	Tapered	1560.88	2.180	15.60	2.65	[140]
	Bi_2Te_3	Sandwich	1558.46	3.220 ns	1.70	7.42	[84]
	Bi_2Se_3	Sandwich	1564.60	1.570	1.21	–	[95]
	Bi_2Se_3	Sandwich	1532.00	1.700	38.72	–	[141]
	Bi_2Se_3	Sandwich	1557.00	0.500	38.72	–	[141]
	Bi_2Se_3	Sandwich	1557.91	7.780 ns	1.71	6.11	[142]
	Bi_2Se_3	Sandwich	1562.40	0.630	22.60	24.76	[94]
	Bi_2Se_3/Mica	Sandwich	1561.95	2.420 ns	1.082	70.78	[143]
	Sb_2Te_3	D-shaped	1556.00	0.449	22.13	77.60	[144]
	Sb_2Te_3	D-shaped	1561.00	0.270	34.58	107.41	[145]
	Sb_2Te_3	Sandwich	1558.50	1.900	3.75	70.18	[146]
	Sb_2Te_3	Tapered	1542.00	0.070	95.40	4716.98	[147]
	Sb_2Te_3	Tapered	1562.71	1.610	13.20	–	[148]
	$Bi_{1.6}Sb_{0.4}Te_3$	Sandwich	1562.02	0.366	35.97	–	[149]
TMDs	MoS_2	D-shaped	1560.00	0.200	14.53	2300.00	[150]
	MoS_2	Sandwich	1564.59	10.840 ns	0.94	12.04	[97]
	WS_2	D-shaped	1557.00	0.660	10.20	–	[151]
	WS_2	Tapered	1540.00	0.067	135.00	–	[101]
	WS_2	Tapered	1557.50	11.000	2.14	603.23	[152]
	WS_2	D-shaped	1557.00	1.320	8.86	9.41	[153]
	WS_2	–	1565.30	2.100	4.20	4195.01	[154]
	WSe_2	Tapered	1557.40	0.164	63.13	2752.74	[155]
	WSe_2	Tapered	1556.42	0.477	14.02	–	[35]
	WSe_2	D-shaped	1556.70	1.310	5.31	0.12	[156]
	$MoSe_2$	D-shaped	1557.10	1.090	5.03	–	[156]
	$MoTe_2$	D-shaped	1561.00	1.200	5.26	–	[157]
	TiS_2	Tapered	1563.30	0.812	22.70	31.16	[158]
	TiS_2	Sandwich	1531.69	2.360	3.43	21.57	[159]
	SnS_2	Tapered	1562.00	1.060	7.19	3.37	[160]
	FeS_2	Tapered	1566.50	1.700	6.40	–	[161]
	$Mo_{0.5}W_{0.5}S_2$	Sandwich	1556.80	0.575	4.87	267.82	[162]
	$ReS_{1.02}Se_{0.98}$	Sandwich	1561.15	0.888	2.95	309.97	[163]
BP		Sandwich	1571.45	0.648	5.96	–	[164]
		Sandwich	1560.70	0.570	6.88	1298.25	[165]
		Tapered	1569.24	0.280	60.50	–	[166]
		–	1562.00	0.635	12.50	–	[167]
		Sandwich	1558.00	0.700	20.82	–	[168]
		Sandwich	1555.00	0.102	23.90	696.08	[103]
		Sandwich	1562.00	0.900	5.66	–	[169]
		Tapered	1576.10	0.404	34.27	136.14	[87]
		Tapered	1562.80	0.291	10.36	431.21	[170]
	PI-BP	Sandwich	1561.00	1.438	5.27	–	[171]
	PVA-BP	Sandwich	1562.00	1.236	5.42	–	[171]
		Sandwich	1567.30	0.538	30.30	–	[172]
MXenes	Ti_3CNT_x	D-shaped	1557.00	0.660	15.40	4.92	[173]
	$Ti_3C_2T_x$	D-shaped	1555.01	0.159	7.28	2578.62	[49]
	$Ti_3C_2T_x$	D-shaped	1567.30	0.946	5.24	–	[92]
	$Ti_3C_2T_x$	Tapered	1550.00	0.104	20.03	624.06	[88]

(Table continued)

SA		Integration	λ/nm	Pulse Width/ps	Repetition Rate/MHz	Peak Power/W	Ref.
	$Ti_3C_2T_x$	Tapered	1566.90	0.650	6.03	–	[104]
	Ti_2CT_x	D-shaped	1565.40	5.300	8.25	–	[174]
	V_2CT_x	Tapered	1559.12	3.210	4.90	–	[105]
	V_2CT_x	Tapered	1560.00	311.000	20.90	0.69	[83]
	Nb_2C	Tapered	1559.00	0.770	14.12	276.24	[175]
	Nb_2C	Tapered	1559.98	0.603	12.54	1296.02	[176]
	Mo_2C	D-shaped	1551.92	0.199	35.74	7610.80	[74]
	Mo_2C	D-shaped	1561.60	0.290	7.90	2981.67	[177]
	Mo_2C/FM	Sandwich	1558.03	0.313	26.80	771.78	[178]
Heterostructures	G–Bi_2Te_3	Sandwich	1565.60	1.170	6.91	–	[179]
	MoS_2–Sb_2Te_3–MoS_2	SAM	1554.00	0.286	36.46	1917.99	[180]
	MoS_2–WS_2	Tapered	1560.00	0.154	74.67	1721.86	[181]
	SnS–CdS	Tapered	1560.80	0.558	34.30	–	[182]
	MoS_2–G	Sandwich	1596.20	1.360	9.80	–	[183]
	Bi_2Te_3–$FeTe_2$	Tapered	1558.80	0.481	23.00	561.33	[184]
	BP–Ti_3C_2	Tapered	1559.80	0.745	11.70	316.64	[185]
	VO_2–V_2O_5	D-shaped	1562.00	0.633	8.10	–	[186]
	G–WS_2	SMF	1566.70	0.357	22.86	1899.27	[187]
	BP-InSe	Tapered	1559.43	0.881	12.69	–	[188]
Graphdiyne		Sandwich	1557.17	0.688	14.60	2001.04	[69]
		Tapered	1564.70	0.734	12.05	165.07	[189]
		Sandwich	1530.70	0.690	14.70	579.71	[190]
		Tapered	1562.90	0.283	9.08	7667.84	[191]
		Tapered	1551.20	0.136	23.50	397.37	[192]
		–	1565.72	0.940	5.05	–	[107]

Table 4. Performance Summary of Mode-Locked Fiber Lasers Based on 2D Layered Materials at 2 μm

SA		Integration	λ/nm	Pulse Width/ps	Repetition Rate/MHz	Peak Power/W	Ref.
Graphene		Sandwich	2060.00	0.190	20.98	13,241.05	[193]
		Sandwich	1913.70	–	19.98	–	[194]
		Sandwich	1908.00	–	1.82	–	[131]
		Sandwich	1945.00	0.205	58.87	1073.17	[195]
		Sandwich	1884.00	1.200	20.50	54.88	[28]
		Sandwich	1940.00	3.600	6.46	111.11	[196]
		Sandwich	1931.90	1.770	12.91	159.41	[197]
		Sandwich	1950.00	0.255	23.50	201.91 kW	[198]
		Sandwich	1931.10	1.770	12.91	–	[197]
TIs	Bi_2Te_3	D-shaped	1935.00	0.795	27.90	–	[199]
	Bi_2Te_3	Tapered	1909.50	1.260	21.50	–	[200]
	Bi_2Se_3	D-typed	1912.12	0.835	18.30	–	[201]
	Sb_2Te_3	Tapered	1930.07	1.240	14.51	7225.27	[202]
	Sb_2Te_3	D-shaped	1961.35	0.890	22.36	4703.42	[203]
TMDs	$MoSe_2$	Sandwich	1943.35	0.980	23.53	397.96	[99]
	$MoSe_2$	D-shaped	1912.00	0.920	18.21	256.67	[204]
	WSe_2	Tapered	1863.96	1.160	11.36	2466.31	[205]
	WSe_2	Tapered	1886.22	1.180	11.36	–	[35]
	WS_2	D-shaped	1941.00	1.300	34.80	13.23	[206]
	WTe_2	Tapered	1915.50	1.250	18.72	1705.13	[207]
	$MoTe_2$	Tapered	1930.22	0.952	14.35	2686.44	[208]
BP		Sandwich	1910.00	0.739	36.80	55.00	[46]
		Tapered	1898.00	1.580	19.20	278.55	[209]
		Sandwich	2094.00	1.300	29.10	291.54	[210]
		Sandwich	1859.30	0.139	20.95	7490.00	[211]
MXenes	$Ti_3C_2T_x$	D-shaped	1913.70	0.897	16.77	830.97	[23]
	Nb_2C	Tapered	1944.00	1.670	9.35	70.45	[212]
	Nb_2C	Tapered	1950.80	1.340	11.76	291.91	[212]
	Nb_2C	Tapered	1882.13	2.270	6.28	862.82	[176]
	V_2C	Tapered	1937.00	1.680	11.52	140.00	[213]
	V_2C	Tapered	1900.00	0.843	18.29	961.83	[214]
Graphdiyne		–	1880.30	2.520	5.94	2431.72	[107]

output power of 172.24 mW in a mode-locked fiber laser using a ferromagnetic insulator $Cr_2Si_2Te_6$ [217]. This is the maximum pulse energy and output power that can be obtained in the 2D material mode-locked fiber laser.

Table 2 shows that various types of 2D materials have been used in fiber lasers in the 1.5 μm band, while graphene is the first 2D material used in mode-locked lasers. As early as 2009, Zhang *et al.* realized a graphene mode-locked fiber laser and obtained a pulse width of 415 fs [130]. Such pioneering studies have shown graphene to be a high-performing SA device with its zero band-gap performance, fast response time, and wide operating interval. In 2020, scientists completed a graphene capacitor-based mode-locked fiber laser [133]. The output performance, using a graphene capacitor integrated into a D-shaped fiber, is shown in Figs. 10(a)–10(c), which demonstrates that the mode-locked laser can switch from femtosecond pulses in reverse to a CW state with an extinction ratio of 70.4 dB. Graphene and its similar derivatives, including graphene oxide and graphene composites, have found applications in fiber mode-locked lasers. Recently, Tsai *et al.* completed a continuous wavelength-tunable fiber mode-locked laser from the C-band around 1544 nm to the L-band around 1574 nm using the combination of a graphene-oxide and nonlinear polarization rotation mechanism [135], and its performance is shown in Figs. 10(d) and 10(e). Of course, in the mid-IR range of 2 μm, graphene also has a notable excellent performance. In 2012, Zhang *et al.* achieved the first graphene-based thulium-doped mode-locked fiber laser with a central wavelength of 1.94 μm, a pulse width of 3.6 ps, and a repetition frequency of 6.46 MHz [196]. This achievement promoted the wide application of graphene at 2 μm. In 2018, Figs. 10(f)–10(g) show that Pawliszewska *et al.* complete the graphene-based holmium-doped mode-locked fiber laser capable of working in a stretched-pulse system, which can generate pulses of 190 fs at 2060 nm [193]. Recently, researchers have prepared a graphene fiber laser that can be mode-locked simultaneously at 1563.5 and 1931.9 nm [197]. The pulse duration is 700 fs and 1.77 ps at a constant pulse repetition rate of 12.905 MHz [Figs. 10(h) and 10(i)]. The completion of this work will facilitate the deployment of several fiber lasers of different wavelengths for practical applications in the near-IR region.

Unlike graphene, TIs have a nonzero band gap and a large modulation depth (up to 95%), especially when using Bi_2Se_3-based SAs, where the lowest repetition rate (1.21 MHz), the smallest unsaturated loss (0.8 dB), and the highest modulation depth (98%) have been reported, which is illustrated in Fig. 11(a) [95]. Therefore, various TI-based mode-locked fiber lasers have been developed. The shortest pulse width of 70 fs was obtained at 1.5 μm, with Sb_2Te_3 as the SA [147], as shown in Figs. 11(b) and 11(c). The highest repetition rate (3.125 GHz) and the largest harmonic order (200th) [140] were obtained by Jin *et al.* with Bi_2Te_3 as the SA, as shown

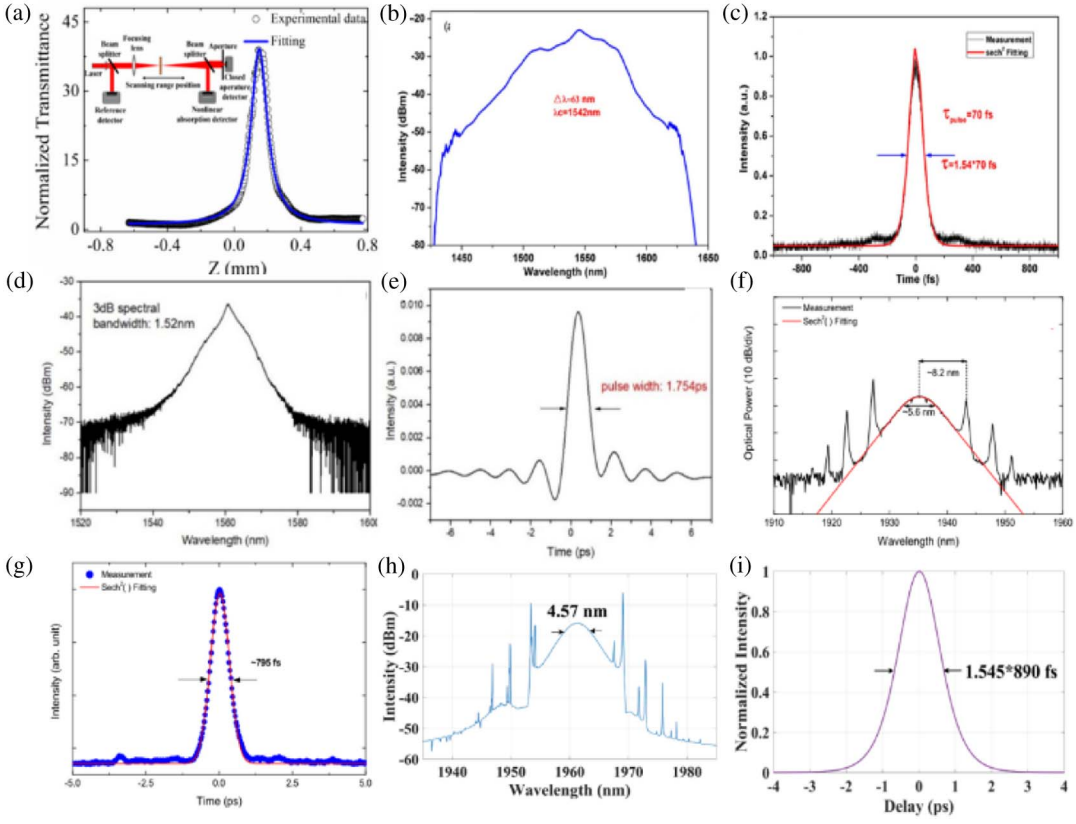

Fig. 11. TIs mode-locked fiber laser at wavelengths of 1.5 μm and 2 μm. (a) Z-scan curves of TIs. Insert: Z-scan experimental setup. (b), (d), and (f) Nonlinear saturable absorption curve. (c), (e), (g), (h), and (i) Autocorrelation trace. (a) Reprinted from Ref. [95], copyright 2012, Optica; (b), (c) reprinted from Ref. [147], copyright 2016, Springer Nature; (d), (e) reprinted from Ref. [140], copyright 2018, Optica; (f), (g) reprinted from Ref. [199], copyright 2014, Optica.

in Figs. 10(d) and 10(e). Note that they used microfiber-based TI SAs and obtained pulses at 1560.88 nm with a pulse width and heavy frequency of 2.18 ps and 15.6 MHz, respectively, when the output power reached the mode-locking operation of 28 mW. At wavelengths of 2 μm, as early as 2014, Jung *et al.* achieved the first ultrafast mode-locked fiber laser pulse at 1935 nm with a pulse width of 795 fs based on Bi_2Te_3 SAs [199], as shown in Figs. 11(f) and 11(g). Note that scientists have also accomplished mode-locked fiber lasers using Sb_2Te_3 at a central wavelength of 1961.35 nm and obtaining pulse width lengths of 890 fs [203], as shown in Figs. 11(h) and 11(i). Of course, researchers have also accomplished achievements using TIs including but not limited to those in Table 3. These achievements demonstrate that topological insulators have a breathtaking potential for applications in nonlinear photonics beyond electrical and thermal properties.

Not coincidentally, TMDs and their derivatives have also been found to be used in mode-locked fiber lasers and have received a lot of attention from experts in the field of photonics. TMDs are a very large material system; it is said that their applications are also more colorful. Back in 2014, MoS_2 was the first object to be studied, revealing its saturable absorption behavior and applying it to fiber lasers, as shown in Fig. 12(a). These research results have given a strong impetus to the development of MoS_2 research and have led to many more important results in the 1.5 μm region [150], as shown in Figs. 12(b) and 12(c). Similarly, WS_2 also exhibits excellent nonlinear optical properties, not unlike MoS_2. In 2017, Liu *et al.* deposited WS_2 on a tapered fiber by photodeposition and in this way completed a sub-100 fs mode-locked laser with the performance pulse width of 67 fs obtained at a central wavelength of 1540 nm [101], which is the shortest pulse width to date for a TMD-based fiber laser in the field of 1.5 μm [Figs. 12(d) and 12(e)]. Through these efforts, other layered TMDs and their derivatives have also been completed as mode-locked fiber lasers in the 1.5 μm domain. One of them even used $PtSe_2$ as an SA to obtain a repetition frequency of 8.8 GHz, which is also a new record. In the 2 μm region, Wang *et al.* generated for the first time a central wavelength at 1915 nm based on WTe_2 SAs ultrafast laser pulses [207], with a pulse width of 1.25 ps. Many works after this achievement are also not negligible, such as a pulse width of 920 fs and a repetition frequency of 34.8 MHz at a pulse width of 1.3 ps [204,206], from the section of Figs. 12(f)–12(i). These studies show that TMDs have become promising 2D materials for mode-locked lasers and are not inferior to graphene and TIs.

BP, which is often prepared by LPE, is more likely to generate ultrafast lasers in the long near-IR wavelength band compared to graphene. In the central wavelength of 1.5 μm, BP was first applied to mode-locked fiber lasers in 2015 when Chen *et al.* proposed an erbium-doped mode-locked fiber laser based on BP SAs [164] and dissected the relationship between the

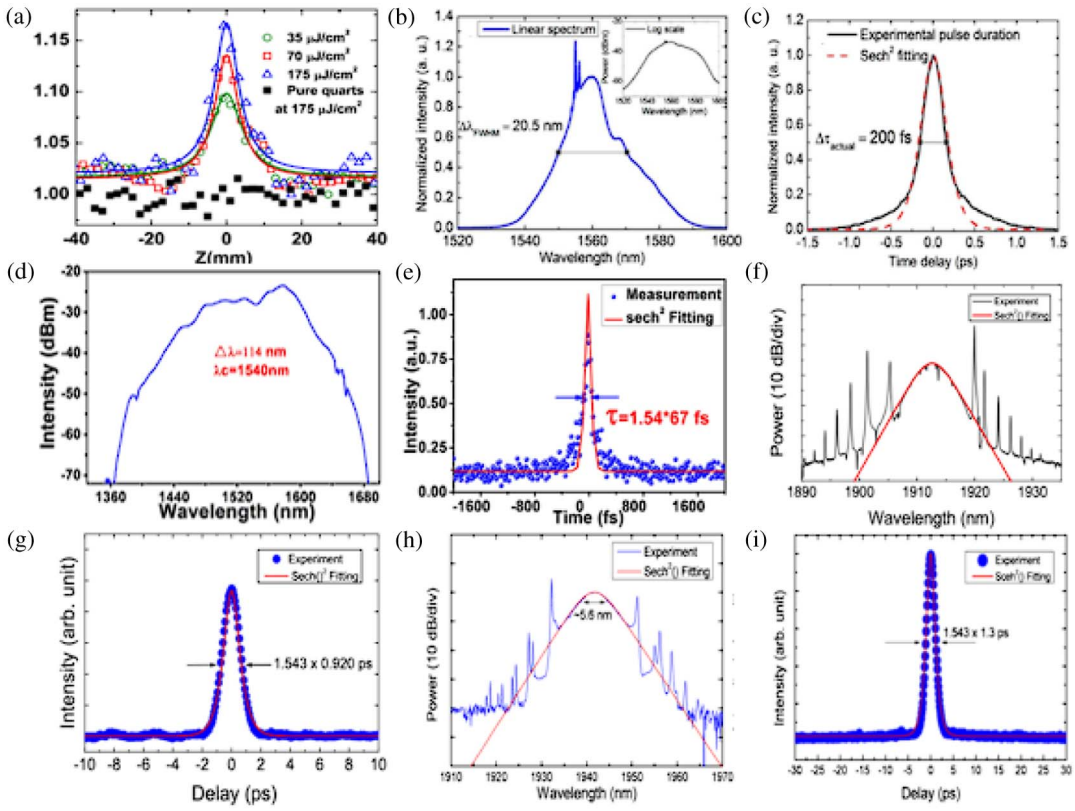

Fig. 12. TMDs mode-locked fiber laser at wavelengths of 1.5 μm and 2 μm. (a) Z-scan measurement of MoS_2; (b), (d), (f), and (h) mode-locked pulses measurements; (c), (e), (g), and (i) AC traces of mode-locked pulses. (a) Reprinted from Ref. [16], copyright 2014, Optica; (b), (c) reprinted from Ref. [150], copyright 2017, Optica; (d), (e) reprinted from Ref. [101], copyright 2017, Optica; (f), (g) reprinted from Ref. [206], copyright 2015, Optica.

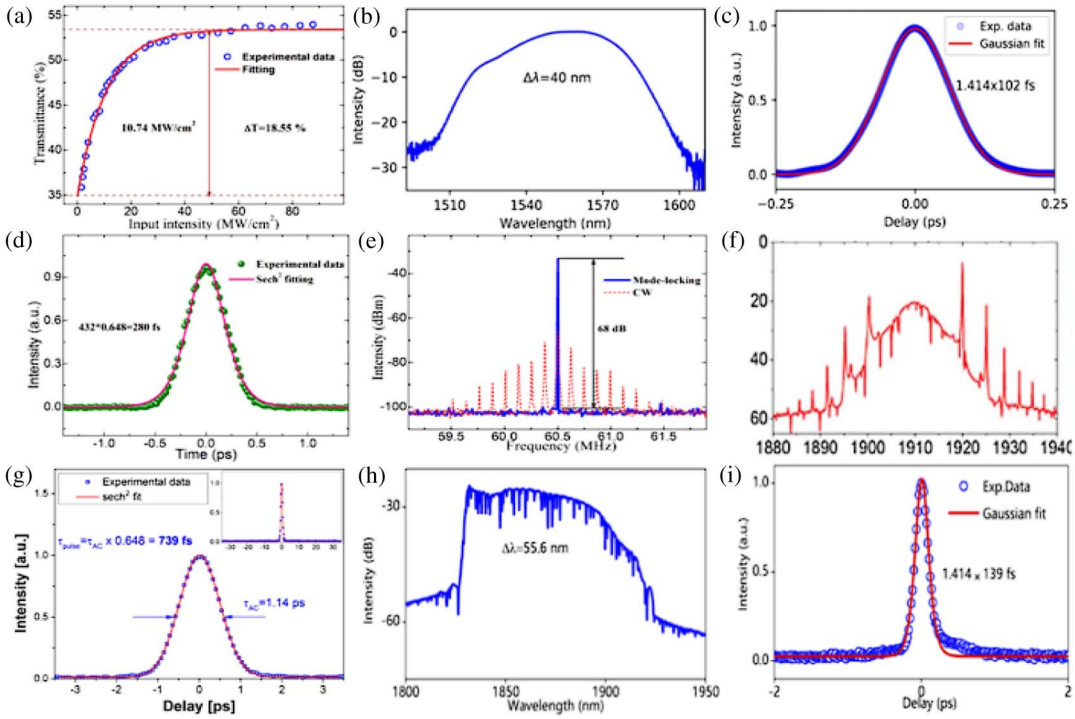

Fig. 13. BP mode-locked fiber laser at wavelengths of 1.5 μm and 2 μm. (a) Relation between the transmittance and input intensity for few-layer BP. (b), (f), and (h) Optical spectra of 1.5 μm and 2 μm. (c), (d), (g), and (i) AC traces of mode-locked pulses. (e) Measured RF spectrum. (a) Reprinted from Ref. [164], copyright 2015, Optica; (b), (c) reprinted from Ref. [103], copyright 2018, Optica; (d), (e) reprinted from Ref. [166], copyright 2016, Optica; (f), (g) reprinted from Ref. [46], copyright 2015, Optica.

transmittance and input intensity of a minority layer BP [Fig. 13(a)]. Thanks to researchers who have been investigating passively mode-locked fiber lasers near 1.5 μm, Jin *et al.* prepared BP sheets using inkjet printing [103], and Zhang *et al.* reported a mode-locked fiber laser with a pulse duration of 102 fs [Fig. 13(c)] based on BP-SA (sandwich structure inkjet-printed), a central wavelength of 1555 nm [Fig. 13(b)], and a BP–SA damage threshold of ~30 mW, which is the narrowest pulse width in the 1.5 μm band among all reported BP-based mode-locked fiber lasers. The characteristics mentioned above can be observed in Figs. 13(b) and 13(c). Not to be neglected, some of the research results are also surprising enough; as shown in Figs. 13(d) and 13(e), excellent data are obtained in experiments with ultrashort pulses of 280 fs and a maximum repetition frequency of 60.5 MHz [166]. On this basis, the soliton center wavelength can be continuously tuned from 1549 to 1575 nm due to the artificial birefringence filtering effect, which also shows that BP can be used as effective SAs to unravel the mystery of soliton dynamics. Of course, mode-locked fiber lasers with 538 fs pulse widths are available in harsher environments [172]. Inkjet-printed BP SAs protected by a parylene-C layer can maintain stability in extreme environments with high temperatures and humidity. For example, at 60°C and with the BP fully immersed in water, it can continue to operate stably for more than 200 hours. Since photodetectors are affected by the conditions and environments in which they are used, this research makes an excellent contribution to the advancement of BP and other 2D materials in real-world applications. These aforementioned studies highlight the excellent nonlinear optical properties of BP as well as its wide tunability range. Similarly, BP exhibits better photon absorption properties than graphene and TMDs in the wavelength region of 2 μm, which is more suitable for the study of a broad bandwidth in the mid-IR short pulse technique. In 2015, Sotor *et al.* experimentally demonstrated for the first time the existence of a thulium-doped mode-locked fiber laser based on BP SAs [46], and obtained an output center wavelength of 1910 nm and a pulse width of 739 fs [Figs. 13(f) and 13(g)]. In 2020, Zhang *et al.* prepared an ultrashort pulse-locked fiber laser based on BP using the dispersion management technique, where the BP was prepared by inkjet printing [211]. As shown in Figs. 13(h) and 13(i), the central wavelength is 1859 nm, and the pulse width is 139 fs, which is the shortest pulse width so far for direct output in BP SAs all-fiber thulium-doped lasers.

MXenes are relatively new 2D materials. Since Ti_3C_2 was prepared as the first MXene material in 2011 [218–220], more than 100 kinds of materials have been unearthed, but less than 50 materials have been applied so far to the experimental field [221]. MXene materials are active at the central wavelength of 1.5 μm, while $Ti_3C_2T_x$ has glamorous optical modulation properties in photonics. In 2019, Wu *et al.* completed a mode-locked fiber laser based on a $Ti_3C_2T_x$ SA in an experiment [88]. A pulse with a central wavelength of 1550 nm and a pulse width of 104 fs was output in a near-zero dispersion (~0.008 ps^2) cavity, and the measured device damage threshold was ~200 mW, which is the narrowest pulse width obtained so far for a mode-locked fiber laser based on a

MXene $Ti_3C_2T_x$ SA [Figs. 14(a)–14(c)]. In addition, significant results were obtained by Liu *et al.* using Mo_2C as SAs [74]. As shown in Figs. 14(d) and 14(e), by adjusting the polarization state and pump power, the pulse duration and output powers are 199 fs and 54.13 mW, respectively, at a wavelength of 1551.92 nm. On the other hand, Jhon *et al.* accomplished a mode-locked laser in the 2 μm region using hundreds of layers of stacked $Ti_3C_2T_x$ [23], which experimentally produced a duration of 897 fs in a fiber cavity of 1913.7 nm femtosecond pulsed lasers, as depicted in Figs. 14(f) and 14(g). This work provides a good reference for low-cost experimental devices based on MXenes. The final point to note is that Lee *et al.* obtained excellent measurement data using V_2C SAs, as shown in Figs. 14(h) and 14(i), and generated an ultrafast pulsed laser of 1.9 μm with a pulse width of 843 fs by a mode-locked fiber laser [214]. These achievements, without exception, demonstrate the physical properties of MXene materials with a broadband optical response and strong effective nonlinear absorption coefficient.

With the continuous exploration of 2D materials, there is an urgent need for SAs with strong nonlinearity, ultrafast recovery time, and a high damage threshold to be used as a device for higher-power ultrashort pulse lasers. From the available research results, a single 2D material has the advantage of a certain area, but it is also difficult to avoid some limitations of the application. The combination of two or more 2D materials allows new materials to expand the advantageous aspects and avoid the limitations of a single development direction. In fact, this way to construct heterostructures has become mainstream in the field of ultrafast photonics. Comparing Tables 2 and 3, shows that heterostructures are relatively widespread for 1.5 μm mode-locked applications. The current ultrafast lasers based on 2D heterostructures are mainly based on graphene and TMDs, followed by other TIs and BP, mainly due to the wideband response of graphene and its mature preparation process, which is a good substrate material to form good van der Waals contact with other 2D materials prepared by LPE, CVD, or magnetron sputtering. In 2017, Liu *et al.* prepared graphene–BP heterostructures by liquid-phase ultrasonic exfoliation and completed the preparation of mode-locked fiber lasers [222]. A central wavelength of 1531 nm was obtained, and the calculated pulse duration was 148 fs, which exhibited good pulse width compression characteristics, as shown in Figs. 15(a) and 15(b). In addition. Liu *et al.*, prepared MoS_2–WS_2 heterostructures by magnetron sputtering and experimentally completed the mode-locked fiber laser [181]. As Figs. 15(c) and 15(d) show, a pulse width of 154 fs was obtained at a central wavelength of 1560 nm, which is the narrowest pulse width that can be obtained for TMD-based heterostructures. However, the triple-layer heterostructures also

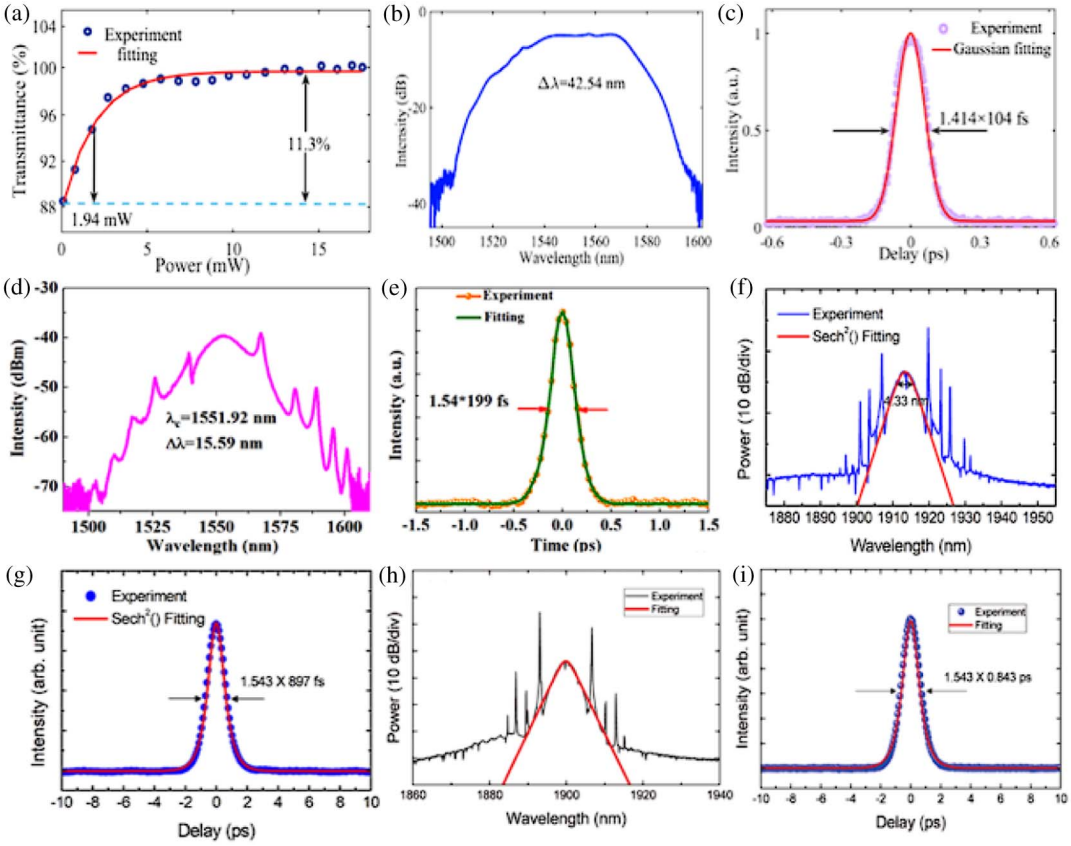

Fig. 14. MXenes mode-locked fiber laser at wavelengths of 1.5 μm and 2 μm. (a) Measured saturable absorption and fitting. (b), (d), (f), and (h) Measured optical spectrum at wavelengths of 1.5 μm and 2 μm. (c), (e), (g), and (i) RF spectrum. (a)–(c) Reprinted from Ref. [88], copyright 2019, Optica; (d), (e) reprinted from Ref. [74], copyright 2021, American Chemical Society; (f), (g) reprinted from Ref. [23], copyright 2021, De Gruyter; (h), (i) reprinted from Ref. [214], copyright 2021, The Royal Society of Chemistry.

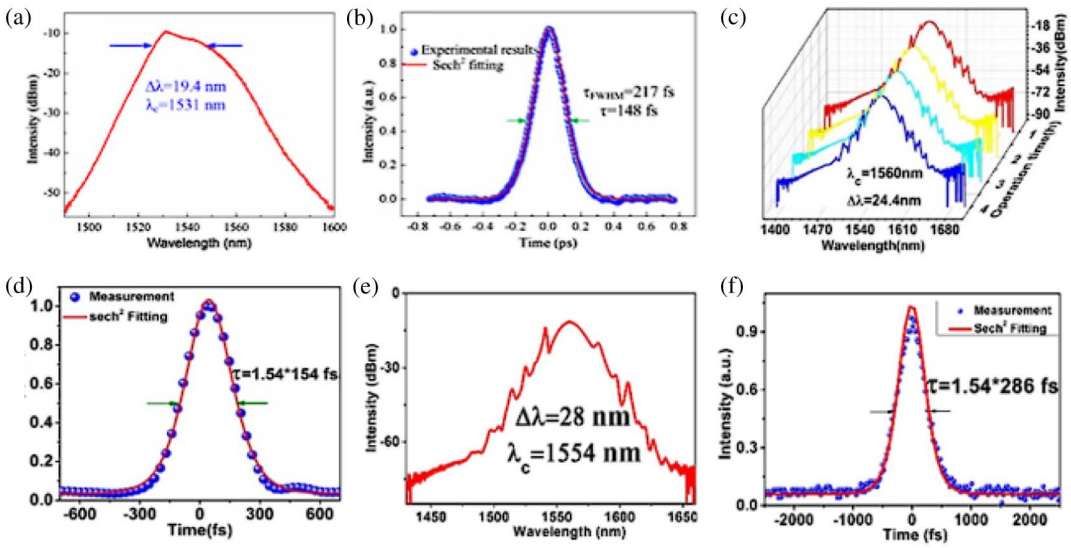

Fig. 15. Heterostructures mode-locked fiber laser at a wavelength of 1.5 μm. (a), (c), and (e) Optical spectrum; (b), (d), and (f) pulse duration. (a), (b) Reprinted from Ref. [222], copyright 2017, Chinese Laser Press; (c), (d) reprinted from Ref. [181], copyright 2019, Optica; (e), (f) reprinted from Ref. [180], copyright 2018, Chinese Laser Press.

exhibit a good narrow pulse width output, and Liu *et al.* prepared a MoS_2–Sb_2Te_3–MoS_2 triple-layer heterojunction by magnetron sputtering and compressed the total thickness of the film to 24 nm [180], as shown in Figs. 15(e) and 15(f). These studies continue to explore the potential of existing materials to improve and apply them to the development in technology and industry. In addition, focusing on the ratio and number of layers in heterostructure materials and exploring their relationship with nonlinear effects can help to further reduce the unsaturated losses of SAs. In the future, we should see heterostructures flourish in the field of ultrafast photonics.

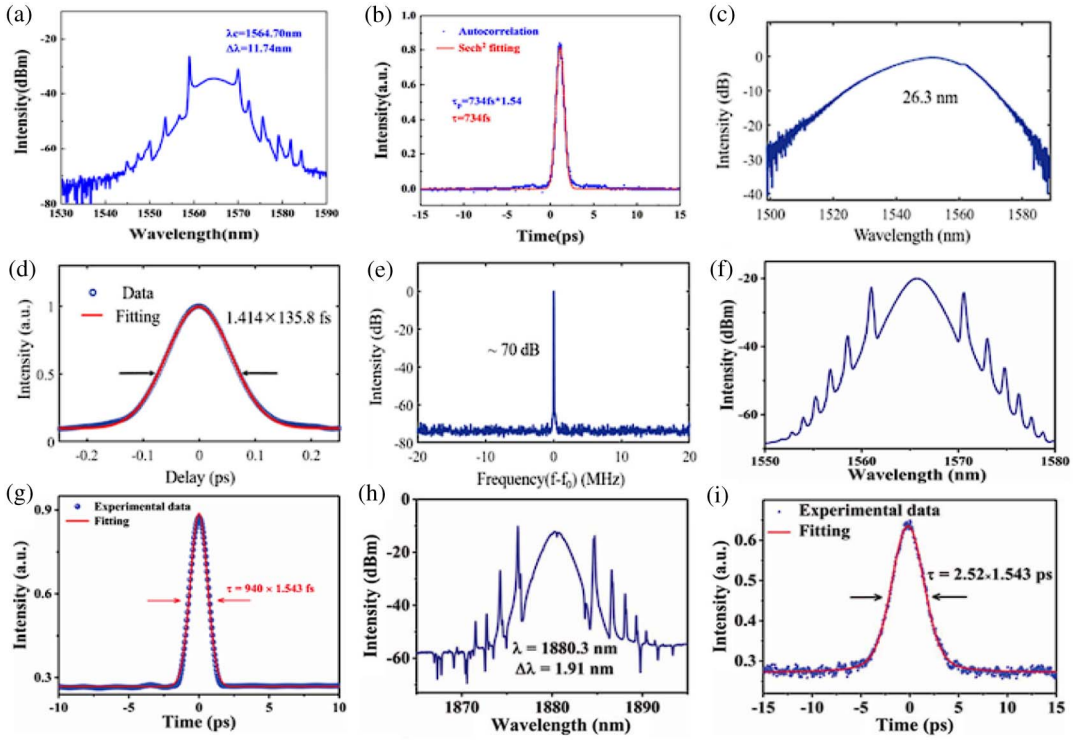

Fig. 16. Performance of GDY-SA-based mode-locked fiber laser performance. (a), (c), (f), and (h) Spectrum of center wavelength. (b), (d), (g), and (i) Autocorrelation trace. (e) RF spectrum with ~70 dB SNR ratio. (a), (b) Reprinted from Ref. [189], copyright 2019, Elsevier; (c)–(e) reprinted from Ref. [192], copyright 2022, MDPI; (f)–(i) reprinted from Ref. [107], copyright 2020, Wiley.

Table 5. Key Parameters for 1.5 μm and 2 μm Mode-Locked Lasers Based on 2D Materials

SA	Type of Laser	Pulse Width/fs	λ/nm	Repetition Rate/MHz	Ref.
Graphene	SL	91	1516	85.16	[110]
G/WS_2	FL	357	1567	22.86	[187]
G-Gold	SL	354	2010	98.00	[113]
Graphene	FL	205	1945	58.87	[195]
Sb_2Te_3	FL	70	1542	95.40	[147]
Bi_2Te_3	FL	795	1935	27.90	[199]
WS_2	FL	67	1540	135.00	[101]
MoS_2	SL	280 ps	2011	232.20	[122]
$MoSe_2$	FL	920	1912	18.21	[204]
BP	SL	9.24 ps	1340	58.14	[126]
BP	FL	102	1555	23.90	[103]
BP	FL	139	1859	20.95	[211]
$Ti_3C_2T_x$	FL	104	1550	20.30	[88]
V_2C	FL	843	1900	18.29	[214]
MoS_2–WS_2	FL	154	1560	74.67	[181]
Graphdiyne	FL	136	1551	23.50	[192]

By applying GDY to a mode-locked fiber laser, a high-power mode-locked pulse output can be achieved. In 2019, Zhao *et al.* obtained a femtosecond mode-locked fiber laser using a GDY SA for the first time [189], obtaining a mode-locked laser pulse of 1564.70 nm with a pulse width of 734 fs [Figs. 16(a) and 16(b)]. This result proves the great promise of GDY for fiber lasers. It is a pity, however, that due to current experimental technology and the cost issues, GDY has not yet been reported to obtain mode-locked laser pulses, but it has successfully achieved a passively *Q*-switched laser in the field of solid-state lasers [106,223–225]. The shortest pulse width of a GDY-based mode-locked fiber laser was obtained by our group in 2022 [192], with a central wavelength of 1551.2 nm, a pulse duration of 135.8 fs, and a repetition frequency of 23.5 MHz, as depicted in Figs. 16(c)–16(e). Note that it is first explored in the field of mid-IR ultrafast photonics using a GDY SA by Guo *et al.* [107]. Not only did they obtain stable mode-locked pulses at 1.5 μm, but also completed a thulium-doped mode-locked fiber laser based on graphdiyne at 1880.30 nm. As shown in Figs. 16(f)–16(i), pulse durations of 940 fs and 2.52 ps were obtained. Graphdiyne has graphene-like properties, but its research in the field of optics is far less intensive than that of graphene. Among the fiber lasers at 1.5 μm, the narrowest pulse width that can be achieved by graphdiyne is 135.8 fs compared to the narrowest pulse width of 390 fs achieved by graphene, which is already better than all the graphene SA fiber lasers recorded in Tables 2 and 3. As shown in the tables, fiber lasers based on a graphdiyne-based SA have a better output performance than most other types of SA.

Comparing Tables 2–4, it is easy to see that the number of reported mode-locked fiber lasers based on 2D materials is more than that of mode-locked solid-state lasers. The main reason is because fiber lasers have a variety of material-coupling methods that can effectively achieve ultrafast mode-locked pulsed lasers using the direct combination of fibers and light, which can meet both the interaction between light and 2D materials and achieve high-power ultrafast laser output. As mentioned above, 2D materials as SAs for solid-state lasers are directly inserted into the cavity, and the light directly interacts with the materials, which causes unnecessary losses and difficulties and limits their widespread use.

4. CONCLUSION AND OUTLOOK

For decades, mode-locked lasers based on 2D nanomaterials have achieved a series of important results because of the continuous in-depth research, and their rapid development has made them gradually become the favorites in the fields of ultrafast photonics and nonlinear optics. With the diversification and maturation of techniques for the preparation and integration of 2D materials and the progress of ultrafast pulsed lasers in recent decades, the combination between the two has become closer and closer, and there has been an unstoppable momentum to design a variety of mode-locked lasers using the nonlinear properties of different 2D materials for practical industrial production and research applications. In this review, we briefly reviewed the development of 2D materials, discussed the material properties, preparation, and testing methods, summarized the laser performance of 2D-based fiber lasers and solid-state lasers in the fields of 1.5 and 2 μm, and provided a detailed summary of the results available so far, highlighting the excellent performance of the lasers. Table 5 summarizes the minimum pulse widths for mode-locked lasers based on 2D materials at 1.5 and 2 μm. For solid-state lasers, the development of mode-locked lasers at 2 μm is still technically and economically limited. For fiber lasers, most thulium-doped mode-locked fiber lasers operate in the soliton-locked state with pulse widths limited to the picosecond magnitude. Researchers have found that dispersion management techniques balance the dispersion and nonlinearity in the laser cavity and, are combined with the cavity design to achieve fs pulse output. Even so, the peak power of current mode-locked fiber lasers based on 2D material SAs is limited by the damage threshold of material substrates, which is difficult to excessively increase. Therefore, the question still remains: how can researchers achieve high-power mode-locked fiber lasers?

In summary, innovative design strategies for devices based on 2D materials mainly include innovations in material preparation, substrate structures, and device integration methods. Ultrafast photonics based on 2D materials has become a highly anticipated field of research. These integration strategies can also be used to prepare devices for many applications in different fields; for example, photodetectors [226–228], all-optical modulators [229–231], and sensors [230,232]. As device preparation techniques improve and integration strategies are updated, we believe devices based on 2D materials will bring revolutionary achievements in biology, optoelectronics, medical devices, and energy.

Funding. National Natural Science Foundation of China (62205091, 61671190); China Postdoctoral Science Foundation (2022M710983); Heilongjiang Provincial Postdoctoral Science Foundation (LBH-Z22201); Fundamental Research Fundation for Universities of Heilongjiang Province (2022-KYYWF-0121).

Disclosures. The authors declare no conflicts of interest.

Data Availability. No data were generated in the presented research.

REFERENCES

1. R. Arora, G. I. Petrov, J. A. Liu, and V. V. Yakovlev, "Improving sensitivity in nonlinear Raman microspectroscopy imaging and sensing," J. Biomed. Opt. **16**, 021114 (2011).
2. B. Nie, I. Saytashev, A. Chong, H. Liu, S. N. Arkhipov, F. W. Wise, and M. Dantus, "Multimodal microscopy with sub-30 fs Yb fiber laser oscillator," Biomed. Opt. Express **3**, 1750–1756 (2012).
3. T. Kurita, K. Komatsuzaki, and M. Hattori, "Advanced material processing with nano- and femto-second pulsed laser," Int. J. Mach. Tools Manuf. **48**, 220–227 (2008).
4. D. Stehr, C. M. Morris, C. Schmidt, and M. S. Sherwin, "High-performance fiber-laser-based terahertz spectrometer," Opt. Lett. **35**, 3799–3801 (2010).
5. R. Ma, W. L. Zhang, S. S. Wang, X. Zeng, H. Wu, and Y. J. Rao, "Simultaneous generation of random lasing and supercontinuum in a completely-opened fiber structure," Laser Phys. Lett. **15**, 085111 (2018).
6. D. E. Spence, P. N. Kean, and W. Sibbett, "60-fsec pulse generation from a self-mode-locked Ti:sapphire laser," Opt. Lett. **16**, 42–44 (1991).
7. J. J. Zayhowski and C. Dill, "Diode-pumped passively *Q*-switched picosecond microchip lasers," Opt. Lett. **19**, 1427–1429 (1994).
8. D. J. Jones, S. A. Diddams, J. K. Ranka, A. Stentz, R. S. Windeler, J. L. Hall, and S. T. Cundiff, "Carrier-envelope phase control of femtosecond mode-locked lasers and direct optical frequency synthesis," Science **288**, 635–639 (2000).
9. O. Okhotnikov, A. Grudinin, and M. Pessa, "Ultra-fast fibre laser systems based on SESAM technology: new horizons and applications," New J. Phys. **6**, 177 (2004).
10. Y. J. Shen, X. H. Han, L. J. Li, X. M. Duan, L. Zhou, W. Q. Xie, R. J. Lan, and Y. Q. Yang, "Continuous-wave mode-locked Tm:YAG laser with GaAs-based SESAM," Infrared Phys. Technol. **111**, 103539 (2020).
11. K. S. Novoselov, A. K. Geim, S. V. Morozov, D. Jiang, Y. Zhang, S. V. Dubonos, I. V. Grigorieva, and A. A. Firsov, "Electric field effect in atomically thin carbon films," Science **306**, 666–669 (2004).
12. T. Hasan, Z. P. Sun, F. Q. Wang, F. Bonaccorso, P. H. Tan, A. G. Rozhin, and A. C. Ferrari, "Nanotube-polymer composites for ultrafast photonics," Adv. Mater. **21**, 3874–3899 (2009).
13. Q. L. Bao, H. Zhang, Y. Wang, Z. H. Ni, Y. L. Yan, Z. X. Shen, K. P. Loh, and D. Y. Tang, "Atomic-layer graphene as a saturable absorber for ultrafast pulsed lasers," Adv. Funct. Mater. **19**, 3077–3083 (2009).
14. Z. P. Sun, T. Hasan, F. Torrisi, D. Popa, G. Privitera, F. Q. Wang, F. Bonaccorso, D. M. Basko, and A. C. Ferrari, "Graphene mode-locked ultrafast laser," ACS Nano **4**, 803–810 (2010).
15. F. Torrisi, T. Hasan, W. P. Wu, Z. P. Sun, A. Lombardo, T. S. Kulmala, G. W. Hsieh, S. J. Jung, F. Bonaccorso, P. J. Paul, D. P. Chu, and A. C. Ferrari, "Inkjet-printed graphene electronics," ACS Nano **6**, 2992–3006 (2012).
16. H. Zhang, S. B. Lu, J. Zheng, J. Du, S. C. Wen, D. Y. Tang, and K. P. Loh, "Molybdenum disulfide (MoS_2) as a broadband saturable absorber for ultra-fast photonics," Opt. Express **22**, 7249–7260 (2014).
17. W. D. Tan, C. Y. Su, R. J. Knize, G. Q. Xie, L. J. Li, and D. Y. Tang, "Mode locking of ceramic Nd:yttrium aluminum garnet with graphene as a saturable absorber," Appl. Phys. Lett. **96**, 031106 (2010).
18. L. M. Zhao, D. Y. Tang, H. Zhang, X. Wu, Q. L. Bao, and K. P. Loh, "Dissipative soliton operation of an ytterbium-doped fiber laser mode locked with atomic multilayer graphene," Opt. Lett. **35**, 3622–3624 (2010).
19. G. Y. Li, G. D. Zhang, R. Lou, Y. S. Wang, X. P. Xie, J. Wang, Y. G. Wang, and G. H. Cheng, "Graphene fabrication by using femtosecond pulsed laser and its application on passively *Q*-switched solid-state laser as saturable absorber," IEEE Photon. J. **12**, 1501009 (2020).
20. K. J. Koski, C. D. Wessells, B. W. Reed, J. J. Cha, D. S. Kong, and Y. Cui, "Chemical intercalation of zerovalent metals into 2D layered Bi_2Se_3 nanoribbons," J. Am. Chem. Soc. **134**, 13773–13779 (2012).
21. C. Y. Ma, C. Wang, B. Gao, J. Adams, G. Wu, and H. Zhang, "Recent progress in ultrafast lasers based on 2D materials as a saturable absorber," Appl. Phys. Rev. **6**, 041304 (2019).
22. Y. Zhang, C. Y. Ma, J. L. Xie, H. Agren, and H. Zhang, "Black phosphorus/polymers: status and challenges," Adv. Mater. **33**, 2100113 (2021).
23. Y. I. Jhon, J. Lee, Y. M. Jhon, and J. H. Lee, "Ultrafast mode-locking in highly stacked $Ti_3C_2T_x$ MXenes for 1.9-μm infrared femtosecond pulsed lasers," Nanophotonics **10**, 1741–1751 (2021).
24. Z. Li, C. Cheng, N. Dong, C. Romero, Q. Lu, J. Wang, J. R. V. de Aldana, Y. Tan, and F. Chen, "*Q*-switching of waveguide lasers based on graphene/WS_2 van der Waals heterostructure," Photon. Res. **5**, 406–410 (2017).
25. M. Ozmaian, A. Fathizadeh, M. Jalalvand, M. R. Ejtehadi, and S. M. V. Allaei, "Diffusion self-assembly of C_{60} molecules on monolayer graphyne sheets," Sci. Rep. **6**, 21910 (2016).
26. Q. Chen, J. Zhao, and H. H. Cheng, "Graphene-based assemblies for moist-electric generation," Front. Energy Res. **9**, 738142 (2021).
27. Y. C. Fan, N. H. Shen, F. L. Zhang, Q. Zhao, H. J. Wu, Q. H. Fu, Z. Y. Wei, H. Q. Li, and C. M. Soukoulis, "Graphene plasmonics: a platform for 2D optics," Adv. Opt. Mater. **7**, 1800537 (2019).
28. G. Sobon, J. Sotor, I. Pasternak, A. Krajewska, W. Strupinski, and K. M. Abramski, "Thulium-doped all-fiber laser mode-locked by CVD-graphene/PMMA saturable absorber," Opt. Express **21**, 12797–12802 (2013).
29. J. H. Lin, G. H. Huang, C. H. Ou, K. C. Che, W. R. Liu, S. Y. Tasy, and Y. H. Chen, "*Q*-switched pulse and mode-locked pulse generation from a Yb^{3+}-doped fiber laser based on Bi_2Se_3," IEEE Photon. J. **10**, 1502410 (2018).
30. P. Gao, H. Z. Huang, X. H. Wang, H. G. Liu, J. H. Huang, W. Weng, S. T. Dai, J. H. Li, and W. X. Lin, "Passively *Q*-switched solid-state Tm:YAG laser using topological insulator Bi_2Te_3 as a saturable absorber," Appl. Opt. **57**, 2020–2024 (2018).
31. Z. Q. Niu, T. L. Feng, T. Li, K. J. Yang, J. Zhao, G. Q. Li, D. C. Li, S. Z. Zhao, W. C. Qiao, H. W. Chu, and Y. Z. Liu, "Theoretical and experimental investigations on doubly *Q*-switched Tm:YAP laser with EOM and Sb_2Te_3 nanosheets," Opt. Express **29**, 24684–24694 (2021).
32. Z. Q. Li, Y. X. Zhang, C. Cheng, H. H. Yu, and F. Chen, "6.5 GHz *Q*-switched mode-locked waveguide lasers based on two-dimensional materials as saturable absorbers," Opt. Express **26**, 11321–11330 (2018).
33. C. J. Zhao, H. Zhang, X. Qi, Y. Chen, Z. T. Wang, S. C. Wen, and D. Y. Tang, "Ultra-short pulse generation by a topological insulator based saturable absorber," Appl. Phys. Lett. **101**, 211106 (2012).
34. M. Zhang, G. H. Hu, G. Q. Hu, R. C. T. Howe, L. Chen, Z. Zheng, and T. Hasan, "Yb- and Er-doped fiber laser *Q*-switched with an optically uniform, broadband WS_2 saturable absorber," Sci. Rep. **5**, 17482 (2015).
35. J. D. Yin, J. R. Li, H. Chen, J. T. Wang, P. G. Yan, M. L. Liu, W. J. Liu, W. Lu, Z. H. Xu, W. F. Zhang, J. Z. Wang, Z. P. Sun, and S. C. Ruan, "Large-area highly crystalline WSe_2 atomic layers for ultrafast pulsed lasers," Opt. Express **25**, 30020–30031 (2017).
36. X. C. Su, B. T. Zhang, Y. R. Wang, G. B. He, G. R. Li, N. Lin, K. J. Yang, J. L. He, and S. D. Liu, "Broadband rhenium disulfide optical modulator for solid-state lasers," Photon. Res. **6**, 498–505 (2018).
37. X. L. Sun, B. T. Zhang, Y. L. Li, X. Y. Luo, G. R. Li, Y. X. Chen, C. Q. Zhang, and J. L. He, "Tunable ultrafast nonlinear optical properties of graphene/MoS_2 van der Waals heterostructures and their application in solid-state bulk lasers," ACS Nano **12**, 11376–11385 (2018).
38. A. Afroozeh, E. Akbari, and P. Yupapin, "Recent advance in gas sensing by using two-dimensional transition metal disulfides materials," J. Nanoelectron. Optoelectron. **14**, 1225–1229 (2019).
39. Y. Xiong, H. W. Chen, D. W. Zhang, and P. Zhou, "Electronic and optoelectronic applications based on ReS_2," Phys. Status Solidi RRL **13**, 1800658 (2019).
40. B. Zhao, D. Y. Shen, Z. C. Zhang, P. Lu, M. Hossain, J. Li, B. Li, and X. D. Duan, "2D metallic transition-metal dichalcogenides:

structures, synthesis, properties, and applications," Adv. Funct. Mater. **31**, 2105132 (2021).
41. A. Brown and S. Rundqvist, "Refinement of the crystal structure of black phosphorus," Acta Crystallographica **19**, 684–685 (1965).
42. M. Zhang, Q. Wu, F. Zhang, L. L. Chen, X. X. Jin, Y. W. Hu, Z. Zheng, and H. Zhang, "2D black phosphorus saturable absorbers for ultrafast photonics," Adv. Opt. Mater. **7**, 1800224 (2019).
43. H. C. Jin, S. Xin, C. H. Chuang, W. D. Li, H. Y. Wang, J. Zhu, H. Y. Xie, T. M. Zhang, Y. Y. Wan, Z. K. Qi, W. S. Yan, Y. R. Lu, T. S. Chan, X. J. Wu, J. B. Goodenough, H. X. Ji, and X. F. Duan, "Black phosphorus composites with engineered interfaces for high-rate high-capacity lithium storage," Science **370**, 192–197 (2020).
44. Y. S. Zhang, S. W. Wang, S. L. Chen, Q. L. Zhang, X. Wang, X. L. Zhu, X. H. Zhang, X. Xu, T. F. Yang, M. He, X. Yang, Z. W. Li, X. Chen, M. F. Wu, Y. R. Lu, R. M. Ma, W. Lu, and A. L. Pan, "Wavelength-tunable mid-infrared lasing from black phosphorus nanosheets," Adv. Mater. **32**, 1808319 (2020).
45. L. J. Li, T. X. Li, L. Zhou, J. Y. Fan, Y. Q. Yang, W. Q. Xie, and S. S. Li, "Passively *Q*-switched diode-pumped Tm, Ho:$LuVO_4$ laser with a black phosphorus saturable absorber," Chin. Phys. B **28**, 094205 (2019).
46. J. Sotor, G. Sobon, M. Kowalczyk, W. Macherzynski, P. Paletko, and K. M. Abramski, "Ultrafast thulium-doped fiber laser mode locked with black phosphorus," Opt. Lett. **40**, 3885–3888 (2015).
47. M. Naguib, V. N. Mochalin, M. W. Barsoum, and Y. Gogotsi, "25th Anniversary Article: MXenes: a new family of two-dimensional materials," Adv. Mater. **26**, 992–1005 (2014).
48. N. Liaros, J. Tucek, K. Dimos, A. Bakandritsos, K. S. Andrikopoulos, D. Gournis, R. Zboril, and S. Couris, "The effect of the degree of oxidation on broadband nonlinear absorption and ferromagnetic ordering in graphene oxide," Nanoscale **8**, 2908–2917 (2016).
49. X. T. Jiang, S. X. Liu, W. Y. Liang, S. J. Luo, Z. L. He, Y. Q. Ge, H. D. Wang, R. Cao, F. Zhang, Q. Wen, J. Q. Li, Q. L. Bao, D. Y. Fan, and H. Zhang, "Broadband nonlinear photonics in few-layer MXene $Ti_3C_2T_x$ (T = F, O, or OH)," Laser Photon. Rev. **12**, 1700229 (2018).
50. S. B. Lu, L. L. Miao, Z. N. Guo, X. Qi, C. J. Zhao, H. Zhang, S. C. Wen, D. Y. Tang, and D. Y. Fan, "Broadband nonlinear optical response in multi-layer black phosphorus: an emerging infrared and mid-infrared optical material," Opt. Express **23**, 11183–11194 (2015).
51. Q. Wu, Y. Z. Wang, W. C. Huang, C. Wang, Z. Zheng, M. Zhang, and H. Zhang, "MXene-based high-performance all-optical modulators for actively *Q*-switched pulse generation," Photon. Res. **8**, 1140–1147 (2020).
52. Y. C. Dong, S. Chertopalov, K. Maleski, B. Anasori, L. Y. Hu, S. Bhattacharya, A. M. Rao, Y. Gogotsi, V. N. Mochalin, and R. Podila, "Saturable absorption in 2D Ti_3C_2 MXene thin films for passive photonic diodes," Adv. Mater. **30**, 1705714 (2018).
53. J. C. Lan, J. P. Qiao, W. H. Sung, C. H. Chen, R. H. Jhang, S. H. Lin, L. R. Ng, G. C. Liang, M. Y. Wu, L. W. Tu, C. M. Cheng, H. Liu, and C. K. Lee, "Role of carrier-transfer in the optical nonlinearity of graphene/Bi_2Te_3 heterojunctions," Nanoscale **12**, 16956–16966 (2020).
54. H. Long, J. W. Hu, F. G. Wu, and H. F. Dong, "Ultrafast pulse lasers based on two-dimensional nanomaterial heterostructures as saturable absorber," Acta Phys. Sin. **69**, 188102 (2020).
55. J. S. He, C. Wang, B. Zhou, Y. Zhao, L. L. Tao, and H. Zhang, "2D van der Waals heterostructures: processing, optical properties and applications in ultrafast photonics," Mater. Horiz. **7**, 2903–2921 (2020).
56. Z. H. Hu, X. Liu, P. L. Hernandez-Martinez, S. S. Zhang, P. Gu, W. Du, W. G. Xu, H. V. Demir, H. Y. Liu, and Q. H. Xiong, "Interfacial charge and energy transfer in van der Waals heterojunctions," Infomat **4**, e12290 (2022).
57. Y. Wen, X. S. Zhao, and W. Zhan, "A MoS_2-graphene heterojunction as saturable absorber for passively *Q*-switched mode-locked Nd:GGG laser," Optik **170**, 90–94 (2018).
58. B. Z. Yan, G. R. Li, B. N. Shi, J. T. Liu, H. K. Nie, K. J. Yang, B. T. Zhang, and J. L. He, "2D tellurene/black phosphorus heterojunctions based broadband nonlinear saturable absorber," Nanophotonics **9**, 2593–2602 (2020).
59. M. M. Haley, S. C. Brand, and J. J. Pak, "Carbon networks based on dehydrobenzoannulenes: synthesis of graphdiyne substructures," Angew. Chem. Int. Ed. Engl. **36**, 836–838 (1997).
60. G. X. Li, Y. L. Li, H. B. Liu, Y. B. Guo, Y. J. Li, and D. B. Zhu, "Architecture of graphdiyne nanoscale films," Chem. Commun. **46**, 3256–3258 (2010).
61. M. Y. Zong, Y. Q. Zu, J. Guo, Z. Zhang, J. J. Liu, Y. Q. Ge, J. Liu, and L. B. Su, "Broadband nonlinear optical response of graphdiyne for mid-infrared solid-state lasers," Sci. China-Phys. Mech. Astron. **64**, 294214 (2021).
62. N. Zhang, J. Y. Wu, T. Y. Yu, J. Q. Lv, H. Liu, and X. P. Xu, "Theory, preparation, properties and catalysis application in 2D graphynes-based materials," Front. Phys. **16**, 23201 (2021).
63. X. Chen, X. Jiang, and N. Yang, "Graphdiyne electrochemistry: progress and perspectives," Small **18**, 2201135 (2022).
64. C. Lu, Y. Yang, J. Wang, R. P. Fu, X. X. Zhao, L. Zhao, Y. Ming, Y. Hu, H. Z. Lin, X. M. Tao, Y. L. Li, and W. Chen, "High-performance graphdiyne-based electrochemical actuators," Nat. Commun. **9**, 752 (2018).
65. C. S. Huang, S. L. Zhang, H. B. Liu, Y. J. Li, G. T. Cui, and Y. L. Li, "Graphdiyne for high capacity and long-life lithium storage," Nano Energy **11**, 481–489 (2015).
66. Y. Fang, Y. R. Xue, Y. J. Li, H. D. Yu, L. Hui, Y. X. Liu, C. Y. Xing, C. Zhang, D. Y. Zhang, Z. Q. Wang, X. Chen, Y. Gao, B. L. Huang, and Y. L. Li, "Graphdiyne interface engineering: highly active and selective ammonia synthesis," Angew. Chem. Int. Ed. **59**, 13021–13027 (2020).
67. X. L. Sheng, C. Chen, H. Y. Liu, Z. Y. Chen, Z. M. Yu, Y. X. Zhao, and S. Y. A. Yang, "Two-dimensional second-order topological insulator in graphdiyne," Phys. Rev. Lett. **123**, 256402 (2019).
68. L. M. Wu, Y. Z. Dong, J. L. Zhao, D. T. Ma, W. C. Huang, Y. Zhang, Y. Z. Wang, X. T. Jiang, Y. J. Xiang, J. Q. Li, Y. Q. Feng, J. L. Xu, and H. Zhang, "Kerr nonlinearity in 2D graphdiyne for passive photonic diodes," Adv. Mater. **31**, 1807981 (2019).
69. J. Guo, R. C. Shi, R. Wang, Y. Z. Wang, F. Zhang, C. Wang, H. L. Chen, C. Y. Ma, Z. H. Wang, Y. Q. Ge, Y. F. Song, Z. Q. Luo, D. Y. Fan, X. T. Jiang, J. L. Xu, and H. Zhang, "Graphdiyne-polymer nanocomposite as a broadband and robust saturable absorber for ultrafast photonics," Laser Photon. Rev. **14**, 1900367 (2020).
70. K. Wu, B. H. Chen, X. Y. Zhang, S. F. Zhang, C. S. Guo, C. Li, P. S. Xiao, J. Wang, L. J. Zhou, W. W. Zou, and J. P. Chen, "High-performance mode-locked and *Q*-switched fiber lasers based on novel 2D materials of topological insulators, transition metal dichalcogenides and black phosphorus: review and perspective (invited)," Opt. Commun. **406**, 214–229 (2018).
71. Z. Du, S. Yang, S. Li, J. Lou, S. Zhang, S. Wang, B. Li, Y. Gong, L. Song, X. Zou, and P. M. Ajayan, "Conversion of non-van der Waals solids to 2D transition-metal chalcogenides," Nature **577**, 492–496 (2020).
72. J. Y. Zhao, D. J. Chen, B. Boateng, G. F. Zeng, Y. P. Han, C. Zhen, J. B. Goodenough, and W. D. He, "Atomic interlamellar ion path in polymeric separator enables long-life and dendrite-free anode in lithium ion batteries," J. Power Sources **451**, 227773 (2020).
73. Z. X. Yang, L. F. Gao, H. L. Chen, F. Zhang, Q. Yang, X. H. Ren, S. Z. U. Din, C. Li, J. C. Leng, J. B. Zhang, Z. W. Lin, J. M. Wang, C. L. Li, and H. Zhang, "Broadband few-layer niobium carbide MXene as saturable absorber for solid-state lasers," Opt. Laser Technol. **142**, 107199 (2021).
74. S. C. Liu, S. G. Shang, R. D. Lv, Y. G. Wang, J. Wang, W. Ren, and Y. S. Wang, "Molybdenum carbide buried in D-shaped fibers as a novel saturable absorber device for ultrafast photonics applications," ACS Appl. Mater. Interfaces **13**, 19128–19137 (2021).
75. A. Alagh, F. E. Annanouch, P. Umek, C. Bittencourt, A. Sierra-Castillo, E. Haye, J. F. Colomer, and E. Llobet, "CVD growth of self-assembled 2D and 1D WS_2 nanomaterials for the ultrasensitive detection of NO_2," Sens. Actuators B Chem. **326**, 128813 (2021).
76. L. L. Chen, L. Du, J. Li, L. L. Yang, Q. Yi, and C. J. Zhao, "Dissipative soliton generation from Yb-doped fiber laser modulated by mechanically exfoliated $NbSe_2$," Front. Phys. **8**, 320 (2020).
77. Y. Zu, C. Zhang, X. Guo, W. Liang, J. Liu, L. Su, and H. Zhang, "A solid-state passively *Q*-switched Tm,Gd:CaF_2 laser with a $Ti_3C_2T_x$ MXene absorber near 2 μm," Laser Phys. Lett. **16**, 015803 (2019).
78. X. Liu, Z. Wang, and J. Zhang, "188 ns pulsed Ho:Sc_2SiO_5 laser operating at 2107.2 nm employing a few-layer graphene saturable absorber," Optik **219**, 164637 (2020).

79. N. Cui, F. Zhang, Y. Q. Zhao, Y. P. Yao, Q. G. Wang, L. L. Dong, H. Y. Zhang, S. D. Liu, J. L. Xu, and H. Zhang, "The visible nonlinear optical properties and passively *Q*-switched laser application of a layered $PtSe_2$ material," Nanoscale **12**, 1061–1066 (2020).
80. B. Guo, "2D noncarbon materials-based nonlinear optical devices for ultrafast photonics," Chin. Opt. Lett. **16**, 020004 (2018).
81. M. Guo, L. P. Ma, W. C. Ren, and T. S. Lai, "Control of the ultrafast photo-electronic dynamics of a chemical-vapor-deposited-grown graphene by ozone oxidation," Photon. Res. **8**, 17–23 (2020).
82. Z. Qin, G. Xie, C. Zhao, S. Wen, P. Yuan, and L. Qian, "Mid-infrared mode-locked pulse generation with multilayer black phosphorus as saturable absorber," Opt. Lett. **41**, 56–59 (2016).
83. C. Liu, G. R. Li, Y. R. Wang, X. C. Su, Y. Y. Xie, F. L. Gao, S. Kumar, and B. Y. Zhang, "Near-infrared all-fiber mode-locked laser based on vanadium carbide nanosheets," Optik **260**, 168792 (2022).
84. Q. Wei, K. D. Niu, X. L. Han, H. N. Zhang, C. Zhang, C. Yang, and B. Y. Man, "Large energy pulses generation in a mode-locked Er-doped fiber laser based on CVD-grown Bi_2Te_3 saturable absorber," Opt. Mater. Express **9**, 3535–3545 (2019).
85. B. Zhang, J. Liu, C. Wang, K. Yang, C. Lee, H. Zhang, and J. He, "Recent progress in 2D material-based saturable absorbers for all solid-state pulsed bulk lasers," Laser Photon. Rev. **14**, 1900240 (2019).
86. G. Hu, T. Albrow-Owen, X. Jin, A. Ali, Y. Hu, R. C. T. Howe, K. Shehzad, Z. Yang, X. Zhu, R. I. Woodward, T.-C. Wu, H. Jussila, J.-B. Wu, P. Peng, P.-H. Tan, Z. Sun, E. J. R. Kelleher, M. Zhang, Y. Xu, and T. Hasan, "Black phosphorus ink formulation for inkjet printing of optoelectronics and photonics," Nat. Commun. **8**, 278 (2017).
87. Y. Li, Y. L. He, Y. Cai, S. Q. Chen, J. Liu, Y. Chen, and Y. J. Xiang, "Black phosphorus: broadband nonlinear optical absorption and application," Laser Phys. Lett. **15**, 025301 (2018).
88. Q. Wu, X. Jin, S. Chen, X. Jiang, Y. Hu, Q. Jiang, L. Wu, J. Li, Z. Zheng, M. Zhang, and H. Zhang, "MXene-based saturable absorber for femtosecond mode-locked fiber lasers," Opt. Express **27**, 10159–10170 (2019).
89. Z. Wang, L. Zhan, J. Wu, Z. Zou, L. Zhang, K. Qian, L. He, and X. Fang, "Self-starting ultrafast fiber lasers mode-locked with alcohol," Opt. Lett. **40**, 3699–3702 (2015).
90. C. Y. Ma, P. Yin, K. Khan, A. K. Tareen, R. Huang, J. Du, Y. Zhang, Z. Shi, R. Cao, S. R. Wei, X. Wang, Y. Q. Ge, Y. F. Song, and L. F. Gao, "Broadband nonlinear photonics in few-layer borophene," Small **17**, 2006891 (2021).
91. J. Du, M. Zhang, Z. Guo, J. Chen, X. Zhu, G. Hu, P. Peng, Z. Zheng, and H. Zhang, "Phosphorene quantum dot saturable absorbers for ultrafast fiber lasers," Sci. Rep. **7**, 42357 (2017).
92. J. Li, Z. L. Zhang, L. Du, L. L. Miao, J. Yi, B. Huang, Y. H. Zou, C. J. Zhao, and S. C. Wen, "Highly stable femtosecond pulse generation from a MXene $Ti_3C_2T_x$ (T = F, O, or OH) mode-locked fiber laser," Photon. Res. **7**, 260–264 (2019).
93. E. K. Ng, K. Y. Lau, H. K. Lee, N. M. Yusoff, A. R. Sarmani, M. F. Omar, and M. A. Mahdi, "L-band femtosecond fiber laser based on a reduced graphene oxide polymer composite saturable absorber," Opt. Mater. Express **11**, 59–72 (2021).
94. H. Haris, H. Arof, A. R. Muhammad, C. L. Anyi, S. J. Tan, N. Kasim, and S. W. Harun, "Passively *Q*-switched and mode-locked erbium-doped fiber laser with topological insulator Bismuth Selenide (Bi_2Se_3) as saturable absorber at C-band region," Opt. Fiber Technol. **48**, 117–122 (2019).
95. C. J. Zhao, Y. H. Zou, Y. Chen, Z. T. Wang, S. B. Lu, H. Zhang, S. C. Wen, and D. Y. Tang, "Wavelength-tunable picosecond soliton fiber laser with topological insulator: Bi_2Se_3 as a mode locker," Opt. Express **20**, 27888–27895 (2012).
96. P. G. Yan, R. Y. Lin, S. C. Ruan, A. J. Liu, and H. Chen, "A 2.95 GHz, femtosecond passive harmonic mode-locked fiber laser based on evanescent field interaction with topological insulator film," Opt. Express **23**, 154–164 (2015).
97. P. F. Ma, W. Lin, H. N. Zhang, S. H. Xu, and Z. M. Yang, "High-power large-energy rectangular mode-locked Er-doped fiber laser based on high-damage-threshold MoS_2 saturable absorber," IEEE Photon. J. **11**, 1504312 (2019).
98. K. P. Wang, J. Wang, J. T. Fan, M. Lotya, A. O'Neill, D. Fox, Y. Y. Feng, X. Y. Zhang, B. X. Jiang, Q. Z. Zhao, H. Z. Zhang, J. N. Coleman, L. Zhang, and W. J. Blau, "Ultrafast saturable absorption of two-dimensional MoS_2 nanosheets," ACS Nano **7**, 9260–9267 (2013).
99. M. M. Wu, X. Li, K. Wu, D. D. Wu, S. X. Dai, T. F. Xu, and Q. H. Nie, "All-fiber 2 μm thulium-doped mode-locked fiber laser based on $MoSe_2$-saturable absorber," Opt. Fiber Technol. **47**, 152–157 (2019).
100. C. Cheng, H. L. Liu, Y. Tan, J. R. V. de Aldana, and F. Chen, "Passively *Q*-switched waveguide lasers based on two-dimensional transition metal diselenide," Opt. Express **24**, 10385–10390 (2016).
101. W. J. Liu, L. H. Pang, H. N. Han, M. L. Liu, M. Lei, S. B. Fang, H. Teng, and Z. Y. Wei, "Tungsten disulfide saturable absorbers for 67 fs mode-locked erbium-doped fiber lasers," Opt. Express **25**, 2950–2959 (2017).
102. S. F. Zhang, N. N. Dong, N. McEvoy, M. O'Brien, S. Winters, N. C. Berner, C. Yim, Y. X. Li, X. Y. Zhang, Z. H. Chen, L. Zhang, G. S. Duesberg, and J. Wang, "Direct observation of degenerate two-photon absorption and its saturation in WS_2 and MoS_2 mono layer and few-layer films," ACS Nano **9**, 7142–7150 (2015).
103. X. Jin, G. Hu, M. Zhang, Y. Hu, T. Albrow-Owen, R. C. T. Howe, T.-C. Wu, Q. Wu, Z. Zheng, and T. Hasan, "102 fs pulse generation from a long-term stable, inkjet-printed black phosphorus-mode-locked fiber laser," Opt. Express **26**, 12506–12513 (2018).
104. J. J. Feng, X. H. Li, T. C. Feng, Y. M. Wang, J. Liu, and H. Zhang, "Harmonic mode-locked Er-doped fiber laser by the evanescent field-based MXene $Ti_3C_2T_x$ (T = F, O, or OH) saturable absorber," Ann. Phys. **532**, 1900437 (2019).
105. W. C. Huang, C. Y. Ma, C. Li, Y. Zhang, L. P. Hu, T. T. Chen, Y. F. Tang, J. F. Ju, and H. Zhang, "Highly stable MXene (V_2CT_x)-based harmonic pulse generation," Nanophotonics **9**, 2577–2585 (2020).
106. C. Zhang, Q. Q. Hao, Y. Q. Zu, M. Y. Zong, J. Guo, F. Zhang, Y. Q. Ge, and J. Liu, "Graphdiyne saturable absorber for passively *Q*-switched Ho^{3+}-doped laser," Nanomaterials **10**, 1848 (2020).
107. J. Guo, Z. H. Wang, R. C. Shi, Y. Zhang, Z. W. He, L. F. Gao, R. Wang, Y. Q. Shu, C. Y. Ma, Y. Q. Ge, Y. F. Song, D. Y. Fan, J. L. Xu, and H. Zhang, "Graphdiyne as a promising mid-infrared nonlinear optical material for ultrafast photonics," Adv. Opt. Mater. **8**, 2000067 (2020).
108. J. L. Xu, X. L. Li, J. L. He, X. P. Hao, Y. Yang, Y. Z. Wu, S. D. Liu, and B. T. Zhang, "Efficient graphene *Q* switching and mode locking of 1.34 μm neodymium lasers," Opt. Lett. **37**, 2652–2654 (2012).
109. Y. R. Wang, B. T. Zhang, H. Yang, J. Hou, X. C. Su, Z. P. Sun, and J. L. He, "Passively mode-locked solid-state laser with absorption tunable graphene saturable absorber mirror," J. Lightwave Technol. **37**, 2927–2931 (2019).
110. S. D. D. Cafiso, E. Ugolotti, A. Schmidt, V. Petrov, U. Griebner, A. Agnesi, W. B. Cho, B. H. Jung, F. Rotermund, S. Bae, B. H. Hong, G. Reali, and F. Pirzio, "Sub-100-fs Cr:YAG laser mode-locked by monolayer graphene saturable absorber," Opt. Lett. **38**, 1745–1747 (2013).
111. G. Q. Xie, J. Ma, P. Lv, W. L. Gao, P. Yuan, L. J. Qian, H. H. Yu, H. J. Zhang, J. Y. Wang, and D. Y. Tang, "Graphene saturable absorber for Q-switching and mode locking at 2 μm wavelength [Invited]," Opt. Mater. Express **2**, 878–883 (2012).
112. J. Ma, G. Q. Xie, P. Lv, W. L. Gao, P. Yuan, L. J. Qian, H. H. Yu, H. J. Zhang, J. Y. Wang, and D. Y. Tang, "Graphene mode-locked femtosecond laser at 2 μm wavelength," Opt. Lett. **37**, 2085–2087 (2012).
113. J. Ma, G. Q. Xie, P. Lv, W. L. Gao, P. Yuan, L. J. Qian, U. Griebner, V. Petrov, H. H. Yu, H. J. Zhang, and J. Y. Wang, "Wavelength-versatile graphene-gold film saturable absorber mirror for ultra-broadband mode-locking of bulk lasers," Sci. Rep. **4**, 5016 (2014).
114. J. Liu, Y. G. Wang, Z. S. Qu, L. H. Zheng, L. B. Su, and J. Xu, "Graphene oxide absorber for 2 μm passive mode-locking Tm: $YAlO_3$ laser," Laser Phys. Lett. **9**, 15–19 (2012).
115. H. L. Wan, W. Cai, F. Wang, S. Z. Jiang, S. C. Xu, and J. Liu, "High-quality monolayer graphene for bulk laser mode-locking near 2 μm," Opt. Quantum Electron. **48**, 11 (2016).
116. M. Paris, A. Tyazhev, P. Loiko, R. Soulard, J. L. Doualan, L. Guillemot, A. Braud, T. Godin, P. Camy, and A. Hideur, "Passively

mode-locked diode-pumped Tm,Ho:LiYF$_4$ laser," Laser Phys. Lett. **17**, 045801 (2020).
117. R. Sun, C. Chen, W. J. Ling, Y. N. Zhang, C. P. Kang, and Q. Xu, "Watt-level passively *Q*-switched mode-locked Tm: LuAG laser with graphene oxide saturable absorber," Acta Phys. Sin. **68**, 104207 (2019).
118. A. A. Lagatsky, Z. Sun, T. S. Kulmala, R. S. Sundaram, S. Milana, F. Torrisi, O. L. Antipov, Y. Lee, J. H. Ahn, C. T. A. Brown, W. Sibbett, and A. C. Ferrari, "2 μm solid-state laser mode-locked by single-layer graphene," Appl. Phys. Lett. **102**, 013113 (2013).
119. G. Zhang, Y. G. Wang, J. Wang, and Z. Y. Jiao, "Passively *Q*-switched and mode-locked YVO$_4$/Nd:YVO$_4$/Nd:YVO$_4$ laser based on a MoS$_2$ saturable absorber at 1342.5 nm," Opt. Laser Technol. **109**, 293–296 (2019).
120. L. J. Li, T. Q. Qi, W. Q. Xie, X. N. Yang, L. Zhou, S. C. Li, H. B. Wu, and Y. J. Shen, "A passively mode-locked Tm:YAG laser with a titanium disulfide saturable absorber," Infrared Phys. Technol. **119**, 103942 (2021).
121. W. J. Ling, T. Xia, Z. Dong, Q. Liu, F. P. Lu, and Y. G. Wang, "Passively *Q*-switched mode-locked Tm, Ho:LLF laser with a WS$_2$ saturable absorber," Acta Phys. Sin. **66**, 114207 (2017).
122. L. J. Li, L. Zhou, T. X. Li, X. N. Yang, W. Q. Xie, X. M. Duan, Y. J. Shen, Y. Q. Yang, W. L. Yang, and H. Zhang, "Passive mode-locking operation of a diode-pumped Tm:YAG laser with a MoS$_2$ saturable absorber," Opt. Laser Technol. **124**, 105986 (2020).
123. C. Chen, W. J. Ling, R. Sun, Q. Xu, and Y. N. Zhang, "Watt-level dual-wavelength *Q*-switched mode-locked all-solid-state Tm:CYA laser," Front. Phys. **7**, 252 (2020).
124. X. Zou, Y. X. Leng, Y. Y. Li, Y. Y. Feng, P. X. Zhang, Y. Hang, and J. Wang, "Passively *Q*-switched mode-locked Tm:LLF laser with a MoS$_2$ saturable absorber," Chin. Opt. Lett. **13**, 081405 (2015).
125. C. Zhang, P. G. Ge, X. W. Fan, J. Liu, S. Z. Jiang, Y. Y. Xu, and B. Y. Man, "MoS$_2$ saturable absorber for a *Q*-switched mode-locked 2 μm laser," Laser Phys. **29**, 015803 (2019).
126. X. L. Sun, H. K. Nie, J. L. He, R. W. Zhao, X. C. Su, Y. R. Wang, B. T. Zhang, R. H. Wang, and K. J. Yang, "Passively mode-locked 1.34 μm bulk laser based on few-layer black phosphorus saturable absorber," Opt. Express **25**, 20025–20032 (2017).
127. L. L. Tao, X. W. Huang, J. S. He, Y. J. Lou, L. H. Zeng, Y. H. Li, H. Long, J. B. Li, L. Zhang, and Y. H. Tsang, "Vertically standing PtSe$_2$ film: a saturable absorber for a passively mode-locked Nd:LuVO$_4$ laser," Photon. Res. **6**, 750–755 (2018).
128. J. Ma, H. T. Huang, K. J. Ning, X. D. Xu, G. Q. Xie, L. J. Qian, K. P. Loh, and D. Y. Tang, "Generation of 30 fs pulses from a diode-pumped graphene mode-locked Yb:CaYAlO$_4$ laser," Opt. Lett. **41**, 890–893 (2016).
129. G. Zhao, J. Hou, Y. Z. Wu, J. L. He, and X. P. Hao, "Preparation of 2D MoS$_2$/graphene heterostructure through a monolayer intercalation method and its application as an optical modulator in pulsed laser generation," Adv. Opt. Mater. **3**, 937–942 (2015).
130. H. Zhang, D. Y. Tang, L. M. Zhao, Q. L. Bao, and K. P. Loh, "Large energy mode locking of an erbium-doped fiber laser with atomic layer graphene," Opt. Express **17**, 17630–17635 (2009).
131. B. Fu, Y. Hua, X. S. Xiao, H. W. Zhu, Z. P. Sun, and C. X. Yang, "Broadband graphene saturable absorber for pulsed fiber lasers at 1, 1.5, and 2 μm," IEEE J. Sel. Top. Quantum Electron. **20**, 1100705 (2014).
132. Z. D. Chen, H. Y. Wang, Y. G. Wang, R. D. Lv, X. G. Yang, J. Wang, L. Li, and W. Ren, "Improved optical damage threshold graphene oxide/SiO$_2$ absorber fabricated by sol-gel technique for mode-locked erbium-doped fiber lasers," Carbon **144**, 737–744 (2019).
133. O. Kovalchuk, S. Uddin, S. Lee, and Y. W. Song, "Graphene capacitor-based electrical switching of mode-locking in all-fiberized femtosecond lasers," ACS Appl. Mater. Interfaces **12**, 54005–54011 (2020).
134. F. Ai, X. W. Li, and J. Q. Qian, "Dual-wavelength mode-locked fiber laser based on graphene materials," Eur. Phys. J. Spec. Top. **231**, 643–649 (2021).
135. L. Y. Tsai, Z. Y. Li, J. H. Lin, Y. F. Song, and H. Zhang, "Wavelength tunable passive-mode locked Er-doped fiber laser based on graphene oxide nano-platelet," Opt. Laser Technol. **140**, 106932 (2021).
136. J. Lee, J. Koo, Y. M. Jhon, and J. H. Lee, "A femtosecond pulse erbium fiber laser incorporating a saturable absorber based on bulk-structured Bi$_2$Te$_3$ topological insulator," Opt. Express **22**, 6165–6173 (2014).
137. Y. H. Lin, S. F. Lin, Y. C. Chi, C. L. Wu, C. H. Cheng, W. H. Tseng, J. H. He, C. I. Wu, C. K. Lee, and G. R. Lin, "Using n- and p-type Bi$_2$Te$_3$ topological insulator nanoparticles to enable controlled femtosecond mode-locking of fiber lasers," ACS Photon. **2**, 481–490 (2015).
138. J. Koo, J. Lee, and J. H. Lee, "Integrated fiber-optic device based on a combination of a piezoelectric transducer and a bulk-structured Bi$_2$Te$_3$ topological insulator for *Q*-switched mode-locking of a fiber laser," J. Lightwave Technol. **35**, 2175–2182 (2017).
139. G. B. Jiang, Y. Zhou, L. L. Wang, and Y. Chen, "PMMA sandwiched Bi$_2$Te$_3$ layer as a saturable absorber in mode-locked fiber laser," Adv. Condens. Matter Phys. **2018**, 7578050 (2018).
140. L. Jin, X. H. Ma, H. Zhang, H. W. Zhang, H. L. Chen, and Y. T. Xu, "3 GHz passively harmonic mode-locked Er-doped fiber laser by evanescent field-based nano-sheets topological insulator," Opt. Express **26**, 31244–31252 (2018).
141. K. X. Li, Y. R. Song, J. R. Tian, H. Y. Guoyu, and R. Q. Xu, "Analysis of bound-soliton states in a dual-wavelength mode-locked fiber laser based on Bi$_2$Se$_3$," IEEE Photon. J. **9**, 1400209 (2017).
142. Q. X. Guo, J. Pan, Y. J. Liu, H. P. Si, Z. Y. Lu, X. L. Han, J. J. Gao, Z. T. Zu, H. N. Zhang, and S. Z. Jiang, "Output energy enhancement in a mode-locked Er-doped fiber laser using CVD-Bi$_2$Se$_3$ as a saturable absorber," Opt. Express **27**, 24670–24681 (2019).
143. Q. X. Guo, X. W. Fan, J. J. Gao, X. L. Han, H. N. Zhang, Y. S. Han, and S. Z. Jiang, "Bi$_2$Se$_3$/mica optical modulator for high-energy mode-locked Er-doped fiber laser," Infrared Phys. Technol. **111**, 103453 (2020).
144. J. Boguslawski, J. Sotor, G. Sobon, J. Tarka, J. Jagiello, W. Macherzynski, L. Lipinska, and K. M. Abramski, "Mode-locked Er-doped fiber laser based on liquid phase exfoliated Sb$_2$Te$_3$ topological insulator," Laser Phys. **24**, 105111 (2014).
145. J. Sotor, G. Sobon, K. Grodecki, and K. M. Abramski, "Mode-locked erbium-doped fiber laser based on evanescent field interaction with Sb$_2$Te$_3$ topological insulator," Appl. Phys. Lett. **104**, 251112 (2014).
146. J. Sotor, G. Sobon, W. Macherzynski, and K. M. Abramski, "Harmonically mode-locked Er-doped fiber laser based on a Sb$_2$Te$_3$ topological insulator saturable absorber," Laser Phys. Lett. **11**, 055102 (2014).
147. W. J. Liu, L. H. Pang, H. N. Han, W. L. Tian, H. Chen, M. Lei, P. G. Yan, and Z. Y. Wei, "70-fs mode-locked erbium-doped fiber laser with topological insulator," Sci. Rep. **6**, 19997 (2016).
148. Z. H. Wang, C. Y. Li, J. W. Ye, Z. Wang, and Y. G. Liu, "Generation of harmonic mode-locking of bound solitons in the ultrafast fiber laser with Sb$_2$Te$_3$ saturable absorber on microfiber," Laser Phys. Lett. **16**, 025103 (2019).
149. C. Y. Song, H. Zhang, L. Jin, X. H. Ma, Y. G. Zou, L. L. Shi, and Y. T. Xu, "Study on the energy band regulation of Bi$_2$-xSb$_x$Te$_3$ and its application as mode locking material in low gain ultrafast fiber laser," Adv. Opt. Mater. **8**, 1901618 (2020).
150. E. J. Aiub, D. Steinberg, E. A. T. de Souza, and L. A. M. Saito, "200-fs mode-locked erbium-doped fiber laser by using mechanically exfoliated MoS$_2$ saturable absorber onto D-shaped optical fiber," Opt. Express **25**, 10546–10552 (2017).
151. L. Li, Y. L. Su, Y. G. Wang, X. Wang, Y. S. Wang, X. H. Li, D. Mao, and J. H. Si, "Femtosecond passively Er-doped mode-locked fiber laser with WS$_2$ solution saturable absorber," IEEE J. Sel. Top. Quantum Electron. **23**, 1100306 (2017).
152. B. Guo, S. Li, Y. X. Fan, and P. F. Wang, "Versatile soliton emission from a WS$_2$ mode-locked fiber laser," Opt. Commun. **406**, 66–71 (2018).
153. D. Mao, Y. D. Wang, C. J. Ma, L. Han, B. Q. Jiang, X. T. Gan, S. J. Hua, W. D. Zhang, T. Mei, and J. L. Zhao, "WS$_2$ mode-locked ultrafast fiber laser," Sci. Rep. **5**, 7965 (2015).
154. Z. H. Wang, Z. Wang, Y. G. Liu, R. J. He, S. M. Han, G. D. Wang, G. Yang, and X. Q. Wang, "Noise-like pulses generated from a passively mode-locked fiber laser with a WS$_2$ saturable absorber on microfiber," Laser Phys. Lett. **15**, 085103 (2018).

155. W. J. Liu, M. L. Liu, Y. Y. Ou Yang, H. R. Hou, G. L. Ma, M. Lei, and Z. Y. Wei, "Tungsten diselenide for mode-locked erbium-doped fiber lasers with short pulse duration," Nanotechnology **29**, 174002 (2018).
156. D. Mao, X. Y. She, B. B. Du, D. X. Yang, W. D. Zhang, K. Song, X. Q. Cui, B. Q. Jiang, T. Peng, and J. L. Zhao, "Erbium-doped fiber laser passively mode locked with few-layer WSe_2/$MoSe_2$ nanosheets," Sci. Rep. **6**, 23583 (2016).
157. D. Mao, B. B. Du, D. X. Yang, S. L. Zhang, Y. D. Wang, W. D. Zhang, X. Y. She, H. C. Cheng, H. B. Zeng, and J. L. Zhao, "Nonlinear saturable absorption of liquid-exfoliated molybdenum/tungsten ditelluride nanosheets," Small **12**, 1489–1497 (2016).
158. X. Zhu, S. Chen, M. Zhang, L. Chen, Q. Wu, J. Zhao, Q. Jiang, Z. Zheng, and H. Zhang, "TiS_2-based saturable absorber for ultrafast fiber lasers," Photon. Res. **6**, C44–C48 (2018).
159. X. X. Shang, L. G. Guo, H. N. Zhang, D. W. Li, and Q. Y. Yue, "Titanium disulfide based saturable absorber for generating passively mode-locked and *Q*-switched ultra-fast fiber lasers," Nanomaterials **10**, 1922 (2020).
160. T. C. Feng, D. Zhang, X. H. Li, Q. Abdul, Z. J. Shi, J. B. Lu, P. L. Guo, Y. Zhang, J. S. Liu, and Q. J. Wang, "SnS_2 nanosheets for Er-doped fiber lasers," ACS Appl. Nano Mater. **3**, 674–681 (2020).
161. D. Zhang, C. X. Zhang, X. H. Li, and A. Qyyum, "Layered iron pyrite for ultrafast photonics application," Nanophotonics **9**, 2515–2522 (2020).
162. J. Lei, J. Wang, X. Wang, and Z. Wei, "Ternary 2D $Mo_{(1-x)}W_xS_2$ as a saturable absorber for femtosecond mode-locked all fiber lasers," Opt. Laser Technol. **145**, 107482 (2022).
163. C. X. Dou, W. Wen, J. L. Wang, M. Y. Ma, L. M. Xie, C. H. Ho, and Z. Y. Wei, "Ternary $ReS_{2(1-x)}Se_{2x}$ alloy saturable absorber for passively *Q*-switched and mode-locked erbium-doped all-fiber lasers," Photon. Res. **7**, 283–288 (2019).
164. Y. Chen, G. B. Jiang, S. Q. Chen, Z. N. Guo, X. F. Yu, C. J. Zhao, H. Zhang, Q. L. Bao, S. C. Wen, D. Y. Tang, and D. Y. Fan, "Mechanically exfoliated black phosphorus as a new saturable absorber for both *Q*-switching and mode-locking laser operation," Opt. Express **23**, 12823–12833 (2015).
165. M. H. M. Ahmed, A. A. Latiff, H. Arof, and S. W. Harun, "Ultrafast erbium-doped fiber laser mode-locked with a black phosphorus saturable absorber," Laser Phys. Lett. **13**, 095104 (2016).
166. Y. Chen, S. Q. Chen, J. Liu, Y. X. Gao, and W. J. Zhang, "Sub-300 femtosecond soliton tunable fiber laser with all-anomalous dispersion passively mode locked by black phosphorus," Opt. Express **24**, 13316–13324 (2016).
167. Y. H. Xu, X. F. Jiang, Y. Q. Ge, Z. N. Guo, Z. K. Zeng, Q. H. Xu, H. Zhang, X. F. Yu, and D. Y. Fan, "Size-dependent nonlinear optical properties of black phosphorus nanosheets and their applications in ultrafast photonics," J. Mater. Chem. C **5**, 3007–3013 (2017).
168. L. Yun, "Black phosphorus saturable absorber for dual-wavelength polarization-locked vector soliton generation," Opt. Express **25**, 32380–32385 (2017).
169. W. L. Li, G. W. Chen, G. M. Wang, C. Zeng, and W. Zhao, "Wideband wavelength-tunable ultrafast fiber laser based on black phosphorus saturable absorber," Laser Phys. Lett. **15**, 125102 (2018).
170. M. Liu, X. F. Jiang, Y. R. Yan, X. D. Wang, A. P. Luo, W. C. Xu, and Z. C. Luo, "Black phosphorus quantum dots for femtosecond laser photonics," Opt. Commun. **406**, 85–90 (2018).
171. D. Mao, M. K. Li, X. Q. Cui, W. D. Zhang, H. Lu, K. Song, and J. L. Zhao, "Stable high-power saturable absorber based on polymer-black-phosphorus films," Opt. Commun. **406**, 254–259 (2018).
172. X. X. Jin, G. H. Hu, M. Zhang, T. Albrow-Owen, Z. Zheng, and T. Hasan, "Environmentally stable black phosphorus saturable absorber for ultrafast laser," Nanophotonics **9**, 2445–2449 (2020).
173. Y. I. Jhon, J. Koo, B. Anasori, M. Seo, J. H. Lee, Y. Gogotsi, and Y. M. Jhon, "Metallic MXene saturable absorber for femtosecond mode-locked lasers," Adv. Mater. **29**, 1702496 (2017).
174. J. Yi, L. Du, J. Li, L. L. Yang, L. Y. Hu, S. H. Huang, Y. C. Dong, L. L. Miao, S. C. Wen, V. N. Mochalin, C. J. Zhao, and A. M. Rao, "Unleashing the potential of Ti_2CT_x MXene as a pulse modulator for mid-infrared fiber lasers," 2D Mater. **6**, 045038 (2019).
175. H. Ahmad, R. Ramli, N. Yusoff, S. A. Reduan, A. K. Zamzuri, and K. Thambiratnam, "Performance of Nb_2C MXene coated on tapered fiber as saturable absorber for the generation of mode-locked erbium-doped fiber laser," Infrared Phys. Technol. **114**, 103647 (2021).
176. L. F. Gao, C. Y. Ma, S. R. Wei, A. V. Kuklin, H. Zhang, and H. Agren, "Applications of few-layer Nb_2C MXene: narrow-band photodetectors and femtosecond mode-locked fiber lasers," ACS Nano **15**, 954–965 (2021).
177. S. X. Liu, J. S. Lu, H. F. Huang, N. Xu, J. L. Qu, and Q. Wen, "Ultrafast photonics applications based on evanescent field interactions with 2D molybdenum carbide (Mo_2C)," J. Mater. Chem. C **9**, 6187–6192 (2021).
178. S. C. Liu, Y. G. Wang, R. D. Lv, J. Wang, H. Z. Wang, Y. Wang, and L. N. Duan, "2D molybdenum carbide (Mo_2C)/fluorine mica (FM) saturable absorber for passively mode-locked erbium-doped all-fiber laser," Nanophotonics **9**, 2523–2530 (2020).
179. Z. T. Wang, H. R. Mu, J. Yuan, C. J. Zhao, Q. L. Bao, and H. Zhang, "Graphene-Bi_2Te_3 heterostructure as broadband saturable absorber for ultra-short pulse generation in Er-doped and Yb-doped fiber lasers," IEEE J. Sel. Top. Quantum Electron. **23**, 8800105 (2017).
180. W. Liu, Y.-N. Zhu, M. Liu, B. Wen, S. Fang, H. Teng, M. Lei, L.-M. Liu, and Z. Wei, "Optical properties and applications for MoS_2-Sb_2Te_3-MoS_2 heterostructure materials," Photon. Res. **6**, 220–227 (2018).
181. W. J. Liu, M. L. Liu, B. Liu, R. G. Quhe, M. Lei, S. B. Fang, H. Teng, and Z. Y. Wei, "Nonlinear optical properties of MoS_2-WS_2 heterostructure in fiber lasers," Opt. Express **27**, 6689–6699 (2019).
182. J. J. Feng, X. H. Li, G. Q. Zhu, and Q. J. Wang, "Emerging high-performance SnS/CdS nanoflower heterojunction for ultrafast photonics," ACS Appl. Mater. Interfaces **12**, 43098–43105 (2020).
183. H. H. Liu, Z. L. Li, W. Song, Y. Yu, F. F. Pang, and T. Y. Wang, "MoS_2/graphene heterostructure incorporated passively mode-locked fiber laser: from anomalous to normal average dispersion," Opt. Mater. Express **10**, 46–56 (2020).
184. L. F. Zhang, J. F. Liu, J. Z. Li, Z. Wang, Y. W. Wang, Y. Q. Ge, W. L. Dong, N. Xu, T. C. He, H. Zhang, and W. J. Zhang, "Site-selective Bi_2Te_3-$FeTe_2$ heterostructure as a broadband saturable absorber for ultrafast photonics," Laser Photon. Rev. **14**, 1900409 (2020).
185. X. F. Xia, C. Y. Ma, H. L. Chen, K. Khan, A. K. Tateen, and Q. L. Xiao, "Nonlinear optical properties and ultrafast photonics of 2D BP/Ti_3C_2 heterostructures," Opt. Mater. **112**, 110809 (2021).
186. L. L. Chen, J. Huang, N. Li, H. Zhu, J. B. Hu, L. L. Miao, and C. J. Zhao, "Broadband nonlinear optical modulator enabled by VO_2/V_2O_5 core-shell heterostructures," Nanophotonics **11**, 2931–2938 (2022).
187. B. L. Lu, Y. Fang, C. Y. Lv, M. Qi, H. W. Chen, and J. T. Bai, "Single- and bound-state soliton mode-locked Er-doped fiber laser based on graphene/WS_2 nanocomposites saturable absorber," Infrared Phys. Technol. **121**, 104024 (2022).
188. Y. Shu, Z. Zhong, C. Ma, P. Guo, L. Wu, Z. Lin, X. Yuan, J. Li, W. Chen, and Q. Xiao, "2D BP/InSe heterostructures as a nonlinear optical material for ultrafast photonics," Nanomaterials **12**, 1809 (2022).
189. Y. Zhao, P. L. Guo, X. H. Li, and Z. W. Jin, "Ultrafast photonics application of graphdiyne in the optical communication region," Carbon **149**, 336–341 (2019).
190. Z. J. Shi, X. H. Li, Y. N. Zhang, H. Q. Li, Y. Zhao, P. L. Guo, and Y. X. Guo, "Graphdiyne for ultrashort pulse generation in an erbium-doped hybrid mode-locked fiber laser," Front. Phys. **7**, 150 (2019).
191. W. Z. Ma, P. Yin, M. M. Li, L. Sui, T. S. Wang, Z. Q. Liu, L. Du, W. L. Bao, and Y. Q. Ge, "Graphdiyne-decorated microfiber based soliton and noise-like pulse generation," Nanophotonics **10**, 3967–3977 (2021).
192. Q. Wu, S. Chen, W. L. Bao, and H. B. Wu, "Femtosecond pulsed fiber laser based on graphdiyne-modified tapered fiber," Nanomaterials **12**, 2050 (2022).
193. M. Pawliszewska, T. Martynkien, A. Przewloka, and J. Sotor, "Dispersion-managed Ho-doped fiber laser mode-locked with a graphene saturable absorber," Opt. Lett. **43**, 38–41 (2018).
194. Z. Q. Luo, Y. Y. Li, Y. Z. Huang, M. Zhong, and X. J. Wan, "Graphene mode-locked and *Q*-switched 2-μm Tm/Ho codoped fiber lasers using 1212-nm high-efficient pumping," Opt. Eng. **55**, 081310 (2016).
195. J. Sotor, J. Boguslawski, T. Martynkien, P. Mergo, A. Krajewska, A. Przewloka, W. Strupinski, and G. Sobon, "All-polarization-maintaining,

stretched-pulse Tm-doped fiber laser, mode-locked by a graphene saturable absorber," Opt. Lett. **42**, 1592–1595 (2017).
196. M. Zhang, E. J. R. Kelleher, F. Torrisi, Z. Sun, T. Hasan, D. Popa, F. Wang, A. C. Ferrari, S. V. Popov, and J. R. Taylor, "Tm-doped fiber laser mode-locked by graphene-polymer composite," Opt. Express **20**, 25077–25084 (2012).
197. K. Y. Lau and M. Z. Zulkifli, "1.56 μm and 1.93 μm synchronized mode-locked fiber laser with graphene saturable absorber," Infrared Phys. Technol. **112**, 103606 (2021).
198. G. Sobon, J. Sotor, A. Przewolka, I. Pasternak, W. Strupinski, and K. Abramski, "Amplification of noise-like pulses generated from a graphene-based Tm-doped all-fiber laser," Opt. Express **24**, 20359–20364 (2016).
199. M. Jung, J. Lee, J. Koo, J. Park, Y. W. Song, K. Lee, S. Lee, and J. H. Lee, "A femtosecond pulse fiber laser at 1935 nm using a bulk-structured Bi_2Te_3 topological insulator," Opt. Express **22**, 7865–7874 (2014).
200. K. Yin, B. Zhang, L. Li, T. Jiang, X. F. Zhou, and J. Hou, "Soliton mode-locked fiber laser based on topological insulator Bi_2Te_3 nanosheets at 2 μm," Photon. Res. **3**, 72–76 (2015).
201. J. Lee and J. H. Lee, "Femtosecond Tm-Ho co-doped fiber laser using a bulk-structured Bi_2Se_3 topological insulator," Chin. Phys. B **27**, 094219 (2018).
202. J. T. Wang, J. D. Yin, T. C. He, and P. G. Yan, "Sb_2Te_3 mode-locked ultrafast fiber laser at 1.93 μm," Chin. Phys. B **27**, 084214 (2018).
203. X. H. Ma, W. Chen, L. Tong, S. Q. Liu, W. W. Dai, S. S. Ye, Z. Q. Zheng, Y. Y. Wang, Y. Zhou, W. Zhang, W. T. Fang, X. L. Chen, M. S. Liao, and W. Q. Gao, "Experimental demonstration of harmonic mode-locking in Sb_2Se_3-based thulium-doped fiber laser," Opt. Laser Technol. **143**, 107286 (2021).
204. J. Lee, J. Koo, J. Lee, Y. M. Jhon, and J. H. Lee, "All-fiberized, femtosecond laser at 1912 nm using a bulk-like $MoSe_2$ saturable absorber," Opt. Mater. Express **7**, 2968–2979 (2017).
205. J. T. Wang, W. Lu, J. R. Li, H. Chen, Z. K. Jiang, J. Z. Wang, W. F. Zhang, M. Zhang, I. L. Li, Z. H. Xu, W. J. Liu, and P. G. Yan, "Ultrafast thulium-doped fiber laser mode locked by monolayer WSe_2," IEEE J. Sel. Top. Quantum Electron. **24**, 1100706 (2018).
206. M. Jung, J. Lee, J. Park, J. Koo, Y. M. Jhon, and J. H. Lee, "Mode-locked, 1.94-μm, all-fiberized laser using WS_2-based evanescent field interaction," Opt. Express **23**, 19996–20006 (2015).
207. J. T. Wang, Z. K. Jiang, H. Chen, J. R. Li, J. D. Yin, J. Z. Wang, T. C. He, P. G. Yan, and S. C. Ruan, "Magnetron-sputtering deposited WTe_2 for an ultrafast thulium-doped fiber laser," Opt. Lett. **42**, 5010–5013 (2017).
208. J. T. Wang, H. Chen, Z. K. Jiang, J. D. Yin, J. Z. Wang, M. Zhang, T. C. He, J. Z. Li, P. G. Yan, and S. C. Ruan, "Mode-locked thulium-doped fiber laser with chemical vapor deposited molybdenum ditelluride," Opt. Lett. **43**, 1998–2001 (2018).
209. H. Yu, X. Zheng, K. Yin, X. A. Cheng, and T. Jiang, "Thulium/holmium-doped fiber laser passively mode locked by black phosphorus nanoplatelets-based saturable absorber," Appl. Opt. **54**, 10290–10294 (2015).
210. M. Pawliszewska, Y. Q. Ge, Z. J. Li, H. Zhang, and J. Sotor, "Fundamental and harmonic mode-locking at 2.1 μm with black phosphorus saturable absorber," Opt. Express **25**, 16916–16921 (2017).
211. Q. Zhang, X. X. Jin, G. H. Hu, M. Zhang, Z. Zheng, and T. Hasan, "Sub-150 fs dispersion-managed soliton generation from an all-fiber Tm-doped laser with BP-SA," Opt. Express **28**, 34104–34110 (2020).
212. H. Ahmad, R. Ramli, N. N. Ismail, S. N. Aidit, N. Yusoff, and M. Z. Samion, "Passively mode locked thulium and thulium/holmium doped fiber lasers using MXene Nb_2C coated microfiber," Sci. Rep. **11**, 11652 (2021).
213. H. Ahmad, R. Ramli, S. A. Reduan, M. F. Ismail, and M. Yasin, "Mode-locked thulium/holmium-doped fiber laser with vanadium carbide deposited on tapered fiber," Opt. Fiber Technol. **65**, 102589 (2021).
214. J. Lee, S. Y. Kwon, and J. H. Lee, "Investigation on the nonlinear optical properties of V_2C MXene at 1.9 μm," J. Mater. Chem. C **9**, 15346–15353 (2021).
215. D. G. Purdie, D. Popa, V. J. Wittwer, Z. Jiang, G. Bonacchini, F. Torrisi, S. Milana, E. Lidorikis, and A. C. Ferrari, "Few-cycle pulses from a graphene mode-locked all-fiber laser," Appl. Phys. Lett. **106**, 253101 (2015).
216. J. Koo, J. Park, J. Lee, Y. M. Jhon, and J. H. Lee, "Femtosecond harmonic mode-locking of a fiber laser at 3.27 GHz using a bulk-like, $MoSe_2$-based saturable absorber," Opt. Express **24**, 10575–10589 (2016).
217. Z. Hong, X. Jiang, M. Zhang, H. Zhang, and X. Liu, "High power and large-energy pulse generation in an erbium-doped fiber laser by a ferromagnetic insulator-$Cr_2Si_2Te_6$ saturable absorber," Nanomaterials **12**, 564 (2022).
218. M. Naguib, O. Mashtalir, J. Carle, V. Presser, J. Lu, L. Hultman, Y. Gogotsi, and M. W. Barsoum, "Two-dimensional transition metal carbides," ACS Nano **6**, 1322–1331 (2012).
219. M. Naguib, J. Come, B. Dyatkin, V. Presser, P. L. Taberna, P. Simon, M. W. Barsoum, and Y. Gogotsi, "MXene: a promising transition metal carbide anode for lithium-ion batteries," Electrochem. Commun. **16**, 61–64 (2012).
220. Q. Tang, Z. Zhou, and P. W. Shen, "Are MXenes promising anode materials for Li ion batteries? Computational studies on electronic properties and Li storage capability of Ti_3C_2 and $Ti_3C_2X_2$ (X = F, OH) monolayer," J. Am. Chem. Soc. **134**, 16909–16916 (2012).
221. M. Zhang, Q. Wu, H. L. Chen, Z. Zheng, and H. Zhang, "Fiber-based all-optical modulation based on two-dimensional materials," 2D Mater. **8**, 012003 (2021).
222. S. Liu, Z. Li, Y. Ge, H. Wang, R. Yue, X. Jiang, J. Li, Q. Wen, and H. Zhang, "Graphene/phosphorene nano-heterojunction: facile synthesis, nonlinear optics, and ultrafast photonics applications with enhanced performance," Photon. Res. **5**, 662–668 (2017).
223. Q. Yang, X. Y. Zhang, Z. X. Yang, X. H. Ren, J. Wang, Q. D. Li, X. L. Cui, and X. L. Zhu, "Broadband gamma-graphyne saturable absorber for *Q*-switched solid-state laser," Appl. Phys. Express **12**, 122006 (2019).
224. Y. Q. Zu, J. Guo, Q. Q. Hao, F. Zhang, C. Wang, J. Liu, and B. Wang, "Graphdiyne as a saturable absorber for 2-μm all-solid-state *Q*-switched laser," Sci. China Mater. **64**, 683–690 (2021).
225. X. Q. Liu, J. Guo, L. H. Zheng, J. Liu, Q. Q. Peng, Y. Q. Ge, and J. Xu, "Two-dimensional graphdiyne for passively *Q*-switched Yb^{3+}:Sc_2SiO_5 laser," Microw. Opt. Technol. Lett. **63**, 2292–2296 (2021).
226. S. Chen, R. Cao, X. Chen, Q. Wu, Y. H. Zeng, S. Gao, Z. N. Guo, J. L. Zhao, M. Zhang, and H. Zhang, "Anisotropic plasmonic nanostructure induced polarization photoresponse for MoS_2-based photodetector," Adv. Mater. Interfaces **7**, 1902179 (2020).
227. X. Tang, Y. L. Zheng, B. Cao, Q. Wu, J. H. Liang, W. L. Wang, and G. Q. Li, "GaN nanowire/Nb-doped MoS_2 nanoflake heterostructures for fast UV-visible photodetectors," ACS Appl. Nano Mater. **5**, 4515–4523 (2022).
228. W. C. Huang, C. Y. Xing, Y. Z. Wang, Z. J. Li, L. M. Wu, D. T. Ma, X. Y. Dai, Y. J. Xiang, J. Q. Li, D. Y. Fan, and H. Zhang, "Facile fabrication and characterization of two-dimensional bismuth(III) sulfide nanosheets for high-performance photodetector applications under ambient conditions," Nanoscale **10**, 2404–2412 (2018).
229. C. Wang, Y. Z. Wang, X. T. Jiang, J. W. Xu, W. C. Huang, F. Zhang, J. F. Liu, F. M. Yang, Y. F. Song, Y. Q. Ge, Q. Wu, M. Zhang, H. Chen, J. Liu, and H. Zhang, "MXene $Ti_3C_2T_x$: a promising photothermal conversion material and application in all-optical modulation and all-optical information loading," Adv. Opt. Mater. **7**, 1900060 (2019).
230. Q. Wu, W. C. Huang, Y. Z. Wang, C. Wang, Z. Zheng, H. Chen, M. Zhang, and H. Zhang, "All-optical control of microfiber knot resonator based on 2D Ti_2CT_x MXene," Adv. Opt. Mater. **8**, 1900977 (2020).
231. Q. Wu, S. Chen, Y. Z. Wang, L. M. Wu, X. T. Jiang, F. Zhang, X. X. Jin, Q. Y. Jiang, Z. Zheng, J. Q. Li, M. Zhang, and H. Zhang, "MZI-based all-optical modulator using MXene $Ti_3C_2T_x$ (T = F, O, or OH) deposited microfiber," Adv. Mater. Technol. **4**, 1800532 (2019).
232. R. Wang, Q. Wu, X. T. Jiang, T. J. Fan, J. Guo, C. Wang, F. Zhang, Y. L. Gao, M. Zhang, Z. Q. Luo, and H. Zhang, "A few-layer InSe-based sensitivity-enhanced photothermal fiber sensor," J. Mater. Chem. C **8**, 132–138 (2020).